The Geological Society of America
Field Guide 33
2013

Seismogenic fault-zone processes and heterogeneity recorded by pseudotachylyte: New insights from the Homestake shear zone, Colorado

Joseph L. Allen*
Department of Physical Sciences, Concord University, Athens, West Virginia 24712-1000, USA

Colin A. Shaw
Department of Earth Sciences, Montana State University, Bozeman, Montana 59717, USA

ABSTRACT

This one-day field trip will examine Proterozoic pseudotachylyte and ultramylonite in the Homestake shear zone (HSZ) in the northeastern Sawatch Range of central Colorado. Our ongoing research and geologic mapping shows that the HSZ incorporates a 25-km-long, partitioned system of dip-slip mylonites and ultramylonites and strike-slip to oblique-slip pseudotachylytes and uniquely preserves details of earthquake rupture at the fault-system scale. The HSZ originated as a high-temperature structure during continental assembly at ~1.7 Ga, and was reactivated as a subvertical, transpressional system at ~1.4 Ga under lower temperatures in a mid-crustal, intracontinental setting. The shear zone was seismogenic in this later deformation cycle. The HSZ shows a lateral frictional-plastic strain gradient across a width of 3–4 km, from mylonite and ultramylonite with mutually crosscutting pseudotachylyte, to mylonitic and recrystallized pseudotachylyte, to a system of dispersed pseudotachylyte-bearing fault strands. The broad width of the shear zone and delocalization of seismogenic fault strands suggests the HSZ is an example of a strong-type seismogenic fault. This trip will examine outcrops demonstrating this frictional-plastic strain gradient and discuss implications for coeval plastic flow and earthquake rupture near the base of the seismogenic zone. We also review the petrology and geochemistry of pseudotachylytes as well as the depth and environment of their generation.

*allenj@concord.edu

Allen, J.L., and Shaw, C.A., 2013, Seismogenic fault-zone processes and heterogeneity recorded by pseudotachylyte: New insights from the Homestake shear zone, Colorado, *in* Abbott, L.D., and Hancock, G.S., eds., Classic Concepts and New Directions: Exploring 125 years of GSA discoveries in the Rocky Mountain region: Geological Society of America Field Guide 33, p. 165–183, doi:10.1130/2013.0033(05).

INTRODUCTION

Tectonic pseudotachylytes are fault rocks that contain cataclastic rock and mineral fragments suspended in a disequilibrium melt phase that is widely interpreted to have been generated by fault-surface friction at high-strain rates during earthquake rupture (Sibson, 1973, 1975; Swanson, 1992; Spray, 1995; Di Toro et al., 2009). Pseudotachylytes also form in other environments including the chaotic array of structures formed during meteorite impacts (Reimold, 1998; Reimold and Gibson, 2005; Melosh, 2005; Spray, 2010), along the basal glide planes of sedimentary (Lin et al., 2001) and igneous bedrock landslides (Masch et al., 1985), and on the surfaces of meter-scale blocks subjected to collisional impacts during pyroclastic flow (Grunewald et al., 2000; Schwarzkopf et al., 2001). In addition, pseudotachylyte-like textures and structures have been reported in rhyolitic volcanic conduits associated with lava domes, suggesting viscous magma can preserve a record of shear fracture (Tuffen and Dingwell, 2005).

The origin of pseudotachylytes has been controversial since early workers began to recognize and describe cryptic, aphanitic veins in the early to mid-1800s that were subsequently termed pseudotachylyte nearly a century ago (Spray, 2010). For example, in meteorite impact structures, the environment in which the term was first used (see Reimold, 1998, Spray, 2010 for a review), the relative contribution of melting through friction versus melting by shock is in question (Melosh, 2005; Reimold and Gibson, 2005). Pseudotachylytes in the central impact core are mostly disseminated networks of sub-mm melts not associated with obvious faults (Fiske et al., 1995), whereas the concentric ring assemblage that outlines impact structures includes very thick melts (10^{-1}–10^{2} m) associated with large-displacement faults (e.g., Spray and Thompson, 1995; Spray, 1997). Hypervelocity impact experiments in the laboratory have recognized that pseudotachylyte-like material can be generated in quartz crystals that have been delivered a large shock load (>42 GPa) resulting in strain heating; this supports conjectures that disseminated pseudotachylytes might be a result of shock-induced melting (Fiske et al., 1995), although the possible role of intragranular friction was identified in subsequent impact experiments (Kenkmann et al., 2000).

Similarly, the origin of tectonic pseudotachylytes has been debated. In part, this is because they are somewhat cryptic in the rock record and challenging to recognize at the mesoscopic and microscopic scales, suggesting that they are either rare or rarely recognized. From the 1960s to the 1990s, radically different interpretations regarding the melt source and extent of melting were presented (cf., review by Maddock, 1992), and extensive debate focused on whether they must form exclusively by melting, or if microstructural observations could be explained by extreme mechanical wear leading to ultracataclasis (e.g., Spray, 1995). Theoretical considerations supported by field and microstructural observations inspired Sibson (1973, 1975) to conclude pseudotachylyte could be generated by seismic slip and should record some details of earthquake source mechanics not readily accessible to seismology. Over the past 25 years, artificial pseudotachylytes have been produced by increasingly sophisticated high-velocity rotary shear experiments conducted by different research groups (e.g., Spray, 1987, 1995, 2005; Lin and Shimamoto, 1998; Di Toro et al., 2006, 2011; Niemeijer et al., 2012). The scaled results demonstrate that pseudotachylyte can be generated by friction at a velocity consistent with slip in natural earthquakes (~1–10 m/s), confirming the hypothesis of Sibson (1973, 1975). The experiments of Spray (1995), for example, showed that room temperature samples progressed from fracture, to cataclasis, to mineral surface melting, to generation of a melt phase sprinkled with solid refractory phases such as quartz in just 2 s. This demonstrates that pseudotachylyte is primarily derived from melting of pulverized rock and mineral fragments, rather than melting of the sheared fault surface. In contrast, however, a recent experiment has shown that amorphous pseudotachylyte-like material can be generated from preexisting cataclasites during slow creep experiments (~10^{-7} m/s) under mid-crustal conditions (300 °C; 500 MPa) (Pec et al., 2012). This potentially raises a question as to whether all tectonic, fault-related pseudotachylytes must be generated at seismic slip velocities in nature, or whether they may also form by aseismic creep.

These examples demonstrate that pseudotachylytes form under a wide range of complex conditions. A common problem is that experimental work is challenged to replicate the broad scale of frictional melting observed in nature. At one extreme, frictional melting proceeds on a time scale of milliseconds at the sub-micron scale. At another extreme, it can rapidly fill multi-kilometer-scale areas with melt, from superfaults recording the collapse of impact structures (Spray and Thompson, 1995; Spray, 1997), to substantial sections of tectonic faults (Allen, 2005). The purpose of this trip is to examine tectonic pseudotachylytes at the fault-system scale in the Proterozoic Homestake shear zone (Fig. 1). Our ongoing mapping in the shear zone has delineated a 25-km-long pseudotachylyte system that parallels a subvertical mylonite-ultramylonite-pseudotachylyte zone. We first review the tectonic setting of the Homestake shear zone (HSZ), the petrology and distribution of pseudotachylytes, and the environment of pseudotachylyte generation. We then describe several field stops that illustrate these and other important characteristics of the shear zone. The HSZ represents the largest mapped system of pseudotachylyte-bearing rocks presently known, and provides unique insight into the seismogenic structure of an exhumed transpressional fault system.

TECTONIC SETTING AND OVERVIEW OF SHEAR-ZONE EVOLUTION

Central Colorado lies within a ~1200-km-wide belt of Paleoproterozoic lithosphere that was accreted to the southern margin of the Wyoming craton between ~1800 Ma and ~1600 Ma (Bickford, 1988; Karlstrom and Bowring, 1988; Hoffman, 1989; Whitmeyer and Karlstrom, 2007). This belt comprises a mosaic of juvenile arc terranes with some influence from older material

(Bickford et al., 2008) and can be divided into two provinces on the basis of the age of deformation. The more northerly Yavapai province, in which the field area lies, shows evidence for major orogenic activity before ~1700 Ma followed by a period of exhumation and the subsequent deposition of thick clastic successions in Arizona, northern New Mexico, and southern Colorado (Silver, 1984; Jones et al., 2009). The Mazatzal province was affected by a major orogenic event that deformed both basement rocks and the overlying clastic successions between 1660 Ma and 1600 Ma (Silver, 1965; Amato et al., 2008). The effects of Mazatzal tectonism extended well into the Yavapai province with evidence for post–1700 Ma shortening at least as far north as Salida and Cañon City (Jones et al., 2009).

Following more than 200 m.y. of relative tectonic quiescence, a widespread tectonic and thermal episode affected the lithosphere of the entire southwestern United States between 1450 Ma and 1350 Ma. The most striking manifestation of this episode is granitic plutons that comprise ~20% of the Precambrian exposure throughout the region (Silver et al., 1977; Anderson, 1983). This intrusive event was accompanied by regional metamorphism (Shaw et al., 1999, 2005; Barnhart et al., 2012) and NW-SE shortening (Nyman et al., 1994; Kirby et al., 1995; Shaw et al., 2001; Barnhart et al., 2012). Although the tectonic setting of the ~1400 Ma episode has long been controversial, a growing body of evidence supports an interpretation of intracontinental convergent tectonism with crustal thickening, heating, and plutonism (Barnhart et al., 2012).

Within the field area early high-temperature fabrics characterized by variable degrees of partial melting are folded into steep upright NE-trending folds. This deformation was dated to ~1710–1630 Ma by in situ chemical U-Th-Pb geochronology on monazite (Shaw et al., 2001). These ages are broadly consistent with the late Yavapai and Mazatzal orogenic episodes during the Paleoproterozoic. Younger ages of ~1400 Ma–1375 Ma coinciding with the Mesoproterozoic regional metamorphic event are recorded in monazite rims and some new grains (Shaw et al., 2001). $^{40}Ar/^{39}Ar$ cooling ages of biotite and muscovite also range between 1450 and 1350 Ma consistent with temperatures in excess of ~350 °C (Shaw et al., 2005). Also at this time the St. Kevin batholith (1398 ± 40 Ma; Pearson et al., 1966) was intruded to the south and southwest of the field area along the southwestern extension of the HSZ (Fig. 1).

Perhaps most importantly for this field trip, the main mylonite and by inference, pseudotachylyte zones, formed during this ~1400 Ma tectonothermal event. In contrast to the bimodal distribution of monazite ages in the country rock reflecting monazite growth during Paleoproterozoic orogenic events around 1700 Ma and 1400 Ma, monazite grains within the main mylonite zone exclusively record ages between 1386 Ma and 1375 Ma suggesting complete resetting of the isotope systematics by dynamic recrystallization (Shaw et al., 2001).

These Paleoproterozoic and Mesoproterozoic orogenic events are also recorded by the development of distinct mesoscopic fabrics and microstructures that Shaw et al. (2001) subdivided into four broad deformation cycles (D_1–D_4; Table 1). The first two (D_1–D_2) record early Paleoproterozoic fabrics, partial melting, and the development of steep northeast-trending upright folds. The second two (D_3–D_4) coincide with the regional Mesoproterozoic tectonothermal event and are recorded by the development of mylonite, ultramylonite, and pseudotachylyte during mid-crustal reactivation of the Homestake shear zone. This field trip focuses on pseudotachylytes that we infer to have formed largely during the D_4 episode of deformation.

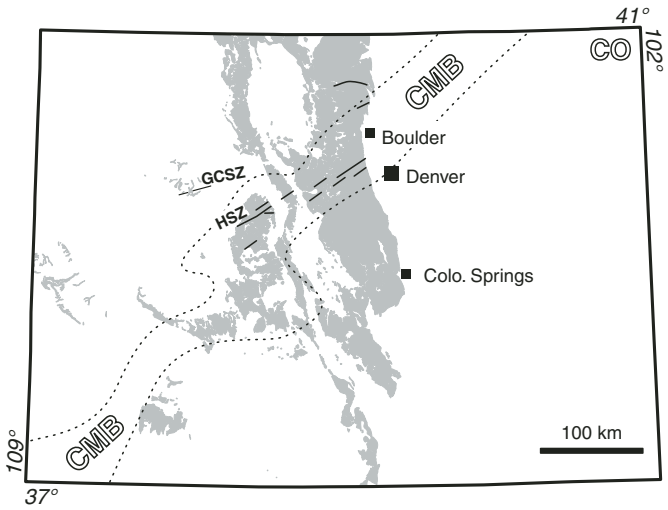

Figure 1. Location map showing outcrop distribution (shaded) of Precambrian rocks in Colorado. Abbreviations: CMB—Colorado mineral belt (Tweto and Sims, 1963; McCoy et al., 2005); HSZ—Homestake shear zone; GCSZ—Grizzly Creek shear zone (cf., Allen and Shaw, 2008, 2011).

PETROLOGY AND GEOCHEMISTRY OF PSEUDOTACHYLYTE AND HOST ROCKS

The primary host rock for pseudotachylyte in the HSZ is a fine- to medium-grained, semi-pelitic gneiss interlayered with coarser-grained pelitic gneiss and schist (Fig. 2A). The stable mineral assemblage consists of quartz + microcline + plagioclase + biotite + magnetite ± sillimanite ± muscovite ± garnet ± cordierite, consistent with upper amphibolite-facies metamorphism at 650–700 °C and 2–5 kbar pressure (Shaw and Allen, 2007). Overall, the semi-pelitic gneiss is silica rich (78.3% SiO_2), and the pelitic interlayers are somewhat less so (69.1%) but more aluminous and Fe-Mg-rich, consistent with their higher biotite and sillimanite content (Table 2). The interlayered gneisses are variably migmatitic and host ribbon-form leucosomes of polycrystalline quartz and alkali feldspar. The leucosome ribbons and micas define a distinct subvertical composite foliation crosscut by irregular leucosomes and thin aplite dikes; this is especially apparent in lower-strain domains where the fabric is less transposed (Fig. 2B). The gneisses locally include 2- to 10-cm-thick lenses of a greenish-gray quartzite that primarily consists of

TABLE 1. SUMMARY OF TECTONIC EVENTS, FABRICS, AND STRUCTURES IN THE HOMESTAKE SHEAR ZONE (HSZ)

Event	Age	Temperature	Structures	Foliation / Lineation / Kinematics
Phanerozoic reactivation	Early Paleozoic and Laramide	Low T	NE-striking brittle faults cutting basement and cover along NE and W flanks of Sawatch Range.	Variable dip slip to strike-slip kinematics on steep, basement-rooted brittle faults concordant to preexisting Proterozoic foliation.
D4	~1380 Ma?	Moderate-T (~300–400°C)	Subvertical ultramylonite in NE-striking shear zones—coeval pseudotachylyte-bearing fault zones.	Subvertical ultramylonite foliation and stretching lineation in shear zones. Ultramylonites dextral SE-side-up; pseudotachylytes dextral strike slip and oblique slip on subvertical faults, and local top-to-SE on steep NW-dipping reverse faults.
D3	~1420–1380 Ma	Moderate-T	Subvertical mylonite in NE-striking shear zones—up to >50-m-wide.	Subvertical mylonite foliation and stretching lineation in shear zones. Mylonites record dextral SE-side-down kinematics.
D2	~1700–1620 Ma	High-T (>500°C)	Upright folds (NE-SW).	Anastomosing high-strain domains within HSZ parallel to axial plane of F_2 folds, subvertical mineral lineation (sil, qtz, bio).
D1	>1710 Ma	High-T	Isoclinal recumbent folding.	Low-angle composite (S_0-S_1) foliation, axial planar to F_1 folds.

Note: cf. Shaw et al. (2001, 2002) for D_1–D_4; Allen (2004) for Phanerozoic.

rounded, fine- to medium-grained, well-sorted quartz grains (Fig. 2C). Very rarely, the pelitic gneiss unit includes minor calcite or dolomite and thin marble lenses. On the basis of these relationships, we interpret the dominant host rock to be a metasedimentary sequence derived from a package of interbedded graywacke and siltstone, with local quartzarenite and subordinate carbonates. D_1–D_2 folding and transposition have overprinted and effectively removed the original stratigraphic order.

In outcrop, pseudotachylyte exists as both fault veins and injection veins (Figs. 2D and 2E). Fault veins separate host rocks that show shear displacement; their traces on outcrop surfaces are commonly linear to broadly curved, concordant to foliation, and have pinch and swell thickness variations. Injection veins branch off of fault veins at moderate to high angles and exhibit displacement consistent with either dilatation normal to the vein walls, or small-scale shear displacement (mm- to cm-scale).

Figure 2. Field images and photomicrographs from the Homestake shear zone (HSZ) showing essential characteristics of supracrustal host rocks and overprinting tectonites. Outcrops are horizontal exposures perpendicular to steep, subvertical foliation; offset markers and Riedel shear geometry suggest most pseudotachylytes are dextral strike slip. (A) Outcrop showing typical interlayered biotite gneiss (top) and pelitic schist (bottom) in transposed D_2 domain; contact at double arrow. The pelitic schist typically hosts coarser leucosomes dominated by quartz-microcline ribbons, and locally includes garnet, cordierite, and 2–8 mm clots of fibrous sillimanite (visible as white wisps in photo). (B) Low-strain domain showing folded leucosomes cut by aplite dike (on left). Field relations are indicative of protracted partial melting and melt migration throughout D_1–D_2. (C) Elongate quartzite lens in biotite gneiss. (D) Pseudotachylyte fault vein with solitary injection veins from the western part of the HSZ. (E) Pseudotachylyte fault vein with light-brown, vein-parallel flow bands, and a complex network of injection veins. (F) Pseudotachylyte fault vein showing flow folds verging toward vein constriction. (G) Pseudotachylyte fault vein concordant to foliation showing sharp boundaries with biotite gneiss (top) and coarse-grained leucosome (bottom). Visible lithic clasts are mostly quartz and polymineralic gneiss fragments. Joints weather to yield a cleated outcrop appearance. (H) Thick concordant fault vein showing numerous large lithic clasts (c), and an intraclast injection (i). Greenish-gray area (w) is a weathered joint surface. Note the rounded character of some clasts indicative of thermal spalling. (I) Plane polarized light (PPL) photomicrograph showing lithic clasts (polymineralic rock fragments and quartz) in opaque matrix. Speckled pattern in matrix is from densely packed, micron-scale magnetite octahedra. Large clast at bottom is part of an 8 mm host-rock fragment with scalloped embayments indicative of partial melting of all mineral grain boundaries, including quartz; matrix above this clast shows a distinct 200-µm-wide flow channel. (J) Photomicrograph using combined PPL and polarized reflected light (PRL). Lithic clasts are quartz (qz) showing some formerly partially melted haloes and silica-rich tails defining primary flow lines, and a 200 µm anhedral magnetite clast (mt) derived from the host rock (as evidenced by the presence of quartz on the right side of the grain). Matrix is packed with ~1–5 µm magnetite microcrysts; this grain size and crystal form is not present in the host rock suggesting they crystallized from the pseudotachylyte melt. (K) PPL photomicrograph showing 450 µm lithic fragment consisting mostly of quartz; a black opaque matrix and a brown matrix are visible. Microprobe energy dispersive spectroscopy spectra show the brown matrix to be slightly enriched in Si and K, and depleted in Fe relative to the black matrix. Note intragranular injection of brown matrix sprinkled with opaque magnetite into brittle crack (inj). (L) PPL photomicrograph showing opaque, dendritic magnetite microlites nucleated on 20 µm magnetite grains (mt) likely derived from the host rock. Note embayed lithic clasts (white) and unidentified acicular microlites. (M) X-ray compositional image from electron microprobe showing backscattered electron image (BSE) combined with distribution of Si and Fe of a magnetite survivor clast (mt) adorned with dendritic magnetite microlites interpreted to have crystallized from the melt. (N) Three X-ray compositional images from electron microprobe of silica-ankerite spheroids (shown with white arrow). Images show BSE overlain by (from left to right), Si/Fe, Si/Mn, and Ti/C.

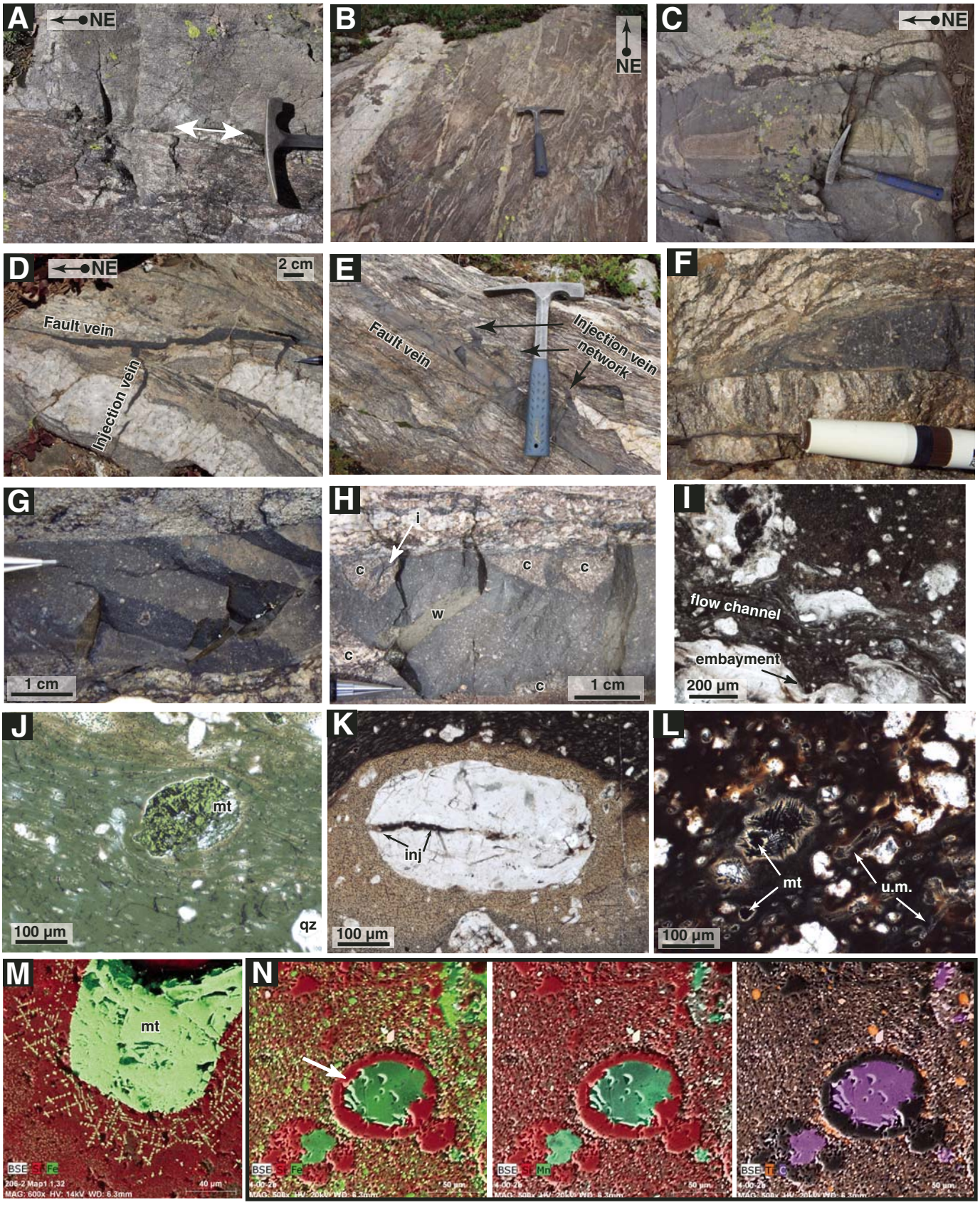
A
NE
B
NE
C
NE
D
NE
2 cm
Fault vein
Injection vein
E
Fault vein
Injection vein network
F
G
1 cm
H
i
c
c
c
w
c
c
1 cm
I
flow channel
embayment
200 µm
J
mt
100 µm
qz
K
inj
100 µm
L
mt
u.m.
100 µm
M
mt
N

TABLE 2. WHOLE-ROCK GEOCHEMISTRY OF BULK PSEUDOTACHYLYTE (WITH LITHIC CLASTS) AND HOST ROCKS FROM THE HOMESTAKE SHEAR ZONE

Sample:	(1) Gneiss 22.3H*	(2) Gneiss 4.1†	(3) Gneiss 15.1†	(4) Gneiss 21.1†	(5) Gneiss 22.1†	(6) Pst Inj. discord. 22.4†	(7) Pst FV discord. 22.3†	(8) Pst FV concord. 39.1†	(9) Gneiss M30.2-10	(10) Pst FV concord. M30.2-10pt	(11) Gneiss 1.4-08	(12) Pst FV concord. 1.4-08pt	(13) Gneiss/ schist 206-93	(14) Pst FV concord. 206-93pt
SiO_2	79.39	79.84	76.66	78.62	79.06	56.30	72.00	66.09	75.92	66.20	78.42	76.57	69.14	63.37
TiO_2	0.60	0.54	0.59	0.68	0.52	1.26	0.80	0.85	0.336	0.992	0.391	0.589	0.868	1.054
Al_2O_3	8.74	8.68	10.30	9.10	9.66	19.78	11.79	15.27	12.51	14.83	10.46	10.85	14.57	16.27
FeO									3.20	7.91	4.60	4.72	6.34	8.05
Fe_2O_3	4.50	4.12	4.59	5.07	4.07	10.21	6.64	7.13						
MnO	0.03	0.06	0.04	0.05	0.04	0.08	0.05	0.06	0.037	0.024	0.069	0.099	0.047	0.055
MgO	0.95	1.14	1.14	1.00	0.99	2.87	1.68	1.90	0.52	1.40	0.89	1.47	1.78	2.02
CaO	1.50	1.11	1.12	0.92	0.92	1.36	1.18	1.09	1.21	0.46	1.18	1.03	0.67	0.62
Na_2O	2.19	2.16	2.45	1.81	2.22	2.49	1.98	2.37	3.66	0.94	2.53	1.84	1.66	0.94
K_2O	1.12	1.41	2.42	2.15	2.33	4.21	2.52	3.34	1.64	4.42	0.99	1.98	3.28	4.48
P_2O_5	0.14	0.02	0.10	0.04	0.08	0.13	0.07	0.10	0.083	0.084	0.066	0.057	0.081	0.109
LOI	0.07	0.48	0.03	0.47	0.47	0.57	1.01	1.38	1.09	2.18	0.61	0.69	1.33	2.51
Oxide total	99.13	99.56	99.55	99.91	99.36	99.26	99.72	99.58	99.12	97.26	99.61	99.20	98.42	96.98
Ni									19	49	19	27	40	49
Cr									78	186	104	109	153	163
Sc									6	19	7	13	17	23
V									47	130	68	82	109	142
Ba		262	459	381	375	510	1080	690	191	726	156	348	945	1112
Rb		70	90	79	116	109	175	163	67	169	42	96	145	200
Sr		171	152	128	139	147	191	153	148	99	115	106	124	117
Zr									159	301	305	234	293	297
Y									18	41	59	27	40	39
Nb									6.9	17.9	6.5	11.5	14.2	20.6
Ga									15	23	15	16	20	25
Cu									3	4	4	2	139	137
Zn									34	69	64	104	89	338
Pb									17	11	11	11	20	22
La									23	45	43	36	48	53
Ce									32	99	89	68	100	117
Th									6	15	14	12	16	17
Nd									13	44	38	29	46	54

Note: Major elements shown as weight-percent oxides; trace elements are parts per million. Columns 9–14 are host rock/pseudotachylyte pairs from the same hand samples; data previously unpublished and analyzed by X-ray fluorescence at Washington State University in 2012. Pst—pseudotachylyte; FV—fault vein; Inj—injection vein; concord—concordant; discord—discordant.

*Data from O'Hara and Huggins (2005).

†Data from Moecher and Sharp (2004); Allen et al. (2002).

Although some injection veins are solitary, most form complex fracture networks asymmetrically localized on one side of a fault vein (Fig. 2E). All vein types are of submillimeter- to decimeter-scale thicknesses and are commonly black to grayish black; some show wispy light-gray to medium-gray or grayish-orange flow bands in the central part of the veins (Fig. 2E). In some of the more weathered exposures, veins show a dusky red surface coloration. The wispy flow bands are almost always associated with thicker veins, where at least part of the vein is >12–14 mm thick. The bands are locally folded into tight to isoclinal folds that typically verge toward thin constrictions and have axial planes subparallel to the vein walls (Fig. 2F), similar to those described by Berlenbach and Roering (1992). Most veins show sharp boundaries with unaltered host rock (Figs. 2D–2H). In some outcrops, thin, foliation-parallel fault veins can be difficult to distinguish from dark biotite selvages and must be examined closely for the presence of thin injections and textural differences in pseudotachylyte, which include subconchoidal fracture, cryptocrystalline matrix, irregularly dispersed lithic clasts, and a subvitreous luster on fresh surfaces.

The petrology and mineralogy of relatively pristine, unmetamorphosed pseudotachylyte are thoroughly described for one location within the Homestake shear zone (Allen et al., 2002; Moecher and Brearley, 2004) from samples in the immediate vicinity of Stops 3 and 4 on this trip. Thin sections from that location show the matrix to be opaque to semi-opaque, brown to black, and aphanitic. The matrix is sprinkled with lithic clasts and mineral fragments derived from the wall rock comprising 15%–40% of the pseudotachylyte by volume (Figs. 2F–2I). These relict fragments are dominated by quartz (~95%), with less common anhedral magnetite, plagioclase feldspar (An_{30}), and alkali feldspar. Accessory monomineralic clasts include allanite, zircon, apatite, monazite, sillimanite, biotite, and hornblende. The latter two hydrous minerals are very rare even though they are primary rock-forming minerals in the host rock, suggesting they have preferentially melted to form the matrix as concluded by many studies of natural and artificial pseudotachylytes (e.g., Maddock, 1992; Magloughlin, 1992; Spray, 1995; Lin and Shimamoto, 1998; Ray, 1999; O'Hara and Sharp, 2001). Polymineralic lithic clasts typically incorporate varying amounts of quartz, plagioclase, alkali feldspar, and magnetite. Sillimanite and biotite are unusual in small polymineralic clasts (<100–200 μm) suggesting they survived melting more frequently in larger clasts.

Microlite phases within the matrix consist of ubiquitous 0.5–5 μm octahedral and dendritic magnetite microcrysts (Figs. 2J–2M), rare micron-scale iron sulfides, and in a single sample, acicular 10–100 μm mullite crystals (Moecher and Brearley, 2004). The dendritic magnetites typically nucleate on survivor magnetite clasts derived from the host rock in thicker veins (>10–12 mm). Most survivor magnetites show an Fe-depleted halo, and those in thicker veins show larger haloes that encompass the length of the magnetite dendrites (Fig. 2M). The haloes lack micron-scale magnetite octahedra, suggesting Fe diffused to form dendrites rather than octahedral microcrysts within the vicinity of magnetite survivors.

The presence of these ubiquitous microcrysts and dendrites provides strong evidence for a melt origin for HSZ pseudotachylytes. Additional evidence for melting includes the presence of concentric silica-carbonate spheroids present in pseudotachylyte cutting carbonate-bearing host rocks. The spheroids are mostly 25–100 μm in size and consist of an outer quartz shell heterogeneously adorned with a thin Ti-rich phase, with an inner core of ankerite (Fig. 2N). Other than the microlites and spheroids, the matrix itself is optically unresolvable. Transmission electron microscopy (TEM) imaging shows that it is dominantly an interlocking mass of 50–500-nm-long phengitic white mica with subordinate quartz, alkali feldspar, rutile, and monazite; the lack of a fabric suggests the mica is a feature of devitrification of the original pseudotachylyte melt (Moecher and Brearley, 2004). In the field trip stop descriptions, we provide additional petrologic observations including the recognition of systematically distributed mylonitic pseudotachylyte in part of the HSZ.

DISTRIBUTION OF PSEUDOTACHYLYTE AT THE FAULT-SYSTEM SCALE

In many pseudotachylyte-bearing fault zones, frictional melting appears to be discontinuous along strike and intimately associated with mappable cataclasite zones (Magloughlin, 1992; Fabbri et al., 2000; Di Toro and Pennacchioni, 2005; Griffith et al., 2008; Smith et al., 2013). Pseudotachylytes in the HSZ differ in that they are concentrated into numerous subparallel, ~5–20-m-wide fault zones for many kilometers along strike, but through-going cataclasites at this scale have not been observed. Importantly, the HSZ does not show a discrete fault core defined by gouge, cataclasites, or retrograde alteration products such as chlorite or epidote.

We subdivide the HSZ into three segments (Fig. 3). The majority of pseudotachylyte in the HSZ is in a system of eight, 1–6-km-long fault strands (the Homestake Creek segment, Fig. 3). Previous work demonstrated that this segment is concordant with a northeast-striking, subvertical foliation in migmatitic supracrustal gneisses, and noted that the volume of pseudotachylyte and the width of each fault zone systematically diminish from southwest to northeast (Allen, 2005). That study also suggested that each of the fault zones formed as a result of long-runout frictional melting, possibly producing at least some pseudotachylyte at the kilometric scale. This interpretation is largely supported by the along-strike persistence of the pseudotachylyte-bearing fault zones and the apparent along-strike continuity of pseudotachylyte fault veins observed within individual outcrops. Furthermore, the Homestake Creek segment shows a predominance of pseudotachylyte in the fault zones as compared to cataclasites, which are less common or absent in some pseudotachylyte-bearing outcrops. Where exposure permits, pseudotachylyte veins can be traced along the entire length of individual outcrops (some exposures are >20–100 m long between covered areas) and appear to

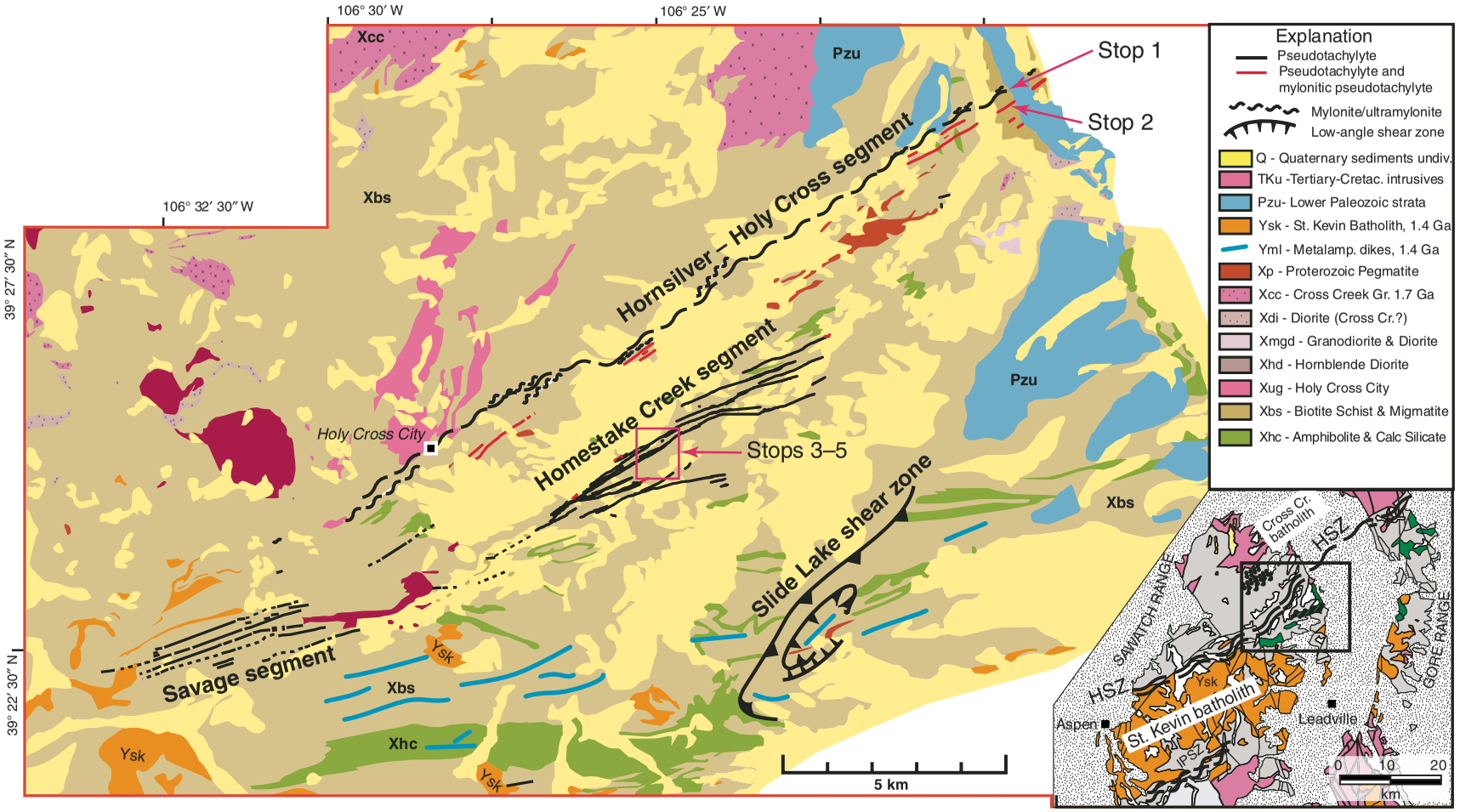

Figure 3. Generalized geologic map of the Homestake shear zone (HSZ) and vicinity highlighting the distribution of mylonite-ultramylonite and pseudotachylyte-bearing fault zones. The deformation history and kinematics are summarized in Table 1 and as follows: (1) the subvertical mylonite-ultramylonite strand in the Hornsilver–Holy Cross segment shows dextral SE-side-down followed by dextral SE-side-up; (2) subvertical pseudotachylyte fault veins in the Homestake Creek segment dominantly show dextral oblique slip to strike slip; and (3) pseudotachylytes of the Savage segment show dextral oblique slip to strike slip on steep faults (70°–90° dips), and local top-to-S displacement on reverse faults oriented ~085°, 60°NW. The Slide Lake shear zone (SLSZ) is a low-angle system that shares similar temperatures, kinematics, and deformation mechanisms with the HSZ suggesting that both systems at least formed at similar crustal levels and in a similar tectonic setting (cf., Lee et al., 2012). Mapping credits: Distribution of pseudotachylyte, mylonite, and ultramylonite by authors; lithologic units modified from Tweto (1974), Wallace et al. (1986), and Wallace and Blaskowski (1989). IPSZ—Independence Pass shear zone. Inset map modified from Tweto et al. (1978).

be continuous pseudotachylyte-bearing faults rather than either: (1) a series of coalescing or overlapping smaller ruptures that sequentially generated pseudotachylyte and grew along strike over time, or (2) a series of longer km-scale faults that generated a mixture of alternating cataclasite and pseudotachylyte along strike. In both cases, the development of more extensive cataclasite zones or a distinctive brittle fault core would be expected.

The Homestake Creek segment parallels a localized mylonite-ultramylonite zone that includes coeval pseudotachylyte and mylonitic pseudotachylyte (the Hornsilver–Holy Cross segment, Fig. 3). The mylonite-ultramylonite zone, originally described by Shaw et al. (2001), is continuous for at least 20 km along strike. The ultramylonite includes some pseudotachylyte and mylonitic pseudotachylyte (Shaw et al., 2001), and was hypothesized to be coeval with pseudotachylytes of the Homestake Creek segment (Shaw and Allen, 2007). New evidence supporting this connection is presented at Stops 1 and 2 on this trip.

The Savage segment is the southwestern extension of the Homestake Creek segment (Fig. 3), and is reported here for the first time. Pseudotachylytes are more dispersed across the width of the Savage segment as compared to the Homestake Creek segment, where they are localized into more discrete and narrow fault zones. The Savage segment represents a distinct bend in the pseudotachylyte system, from 055° to 060° strikes in the Homestake Creek segment to 075° to 100° strikes. It also represents a more varied structural style. On the northwest, pseudotachylytes are commonly preserved as dip-slip faults dipping ~50°–70°NW, whereas on the southeast, pseudotachylytes have steeper dips (75°–85°NW) and exhibit strike-slip to oblique-slip kinematics. Offset markers are uncommon since pseudotachylyte fault veins are mostly concordant to foliation; however, local northwest-striking Riedel shears combined with shallowly plunging slickenlines suggest dextral oblique-slip kinematics are common on subvertical faults throughout the HSZ. Slickenlines with steeper rakes and top-to-SE offsets are common in the ~50°–70° NW dip-slip faults indicating they are reverse faults. The segment is largely exposed in roadless areas along the crest of the Sawatch Range and will not be visited on this field trip.

ENVIRONMENT OF PSEUDOTACHYLYTE GENERATION

As described previously, pseudotachylyte veins typically exhibit sharp boundaries with unaltered gneisses that constitute the vein-bounding wall rock in most of the HSZ. Since most do not systematically overprint cataclasite zones along strike, these field observations suggest that much of the pseudotachylyte formed as first-generation ruptures through intact rock and did not reactivate preexisting brittle faults. This field interpretation is supported by extensive geochemical, isotopic, and mineralogic data that indicate that pseudotachylyte formed in a rock-buffered, closed system, which was not influenced by meteoric fluids. These data include the oxidation state of Fe-bearing phases in matrix microlites (O'Hara and Huggins, 2005) and the oxygen and hydrogen isotope composition of bulk pseudotachylyte matrix (Moecher and Sharp, 2004).

Depth

Field and microstructural evidence suggests the pseudotachylytes formed in a setting coeval with Mesoproterozoic development of ultramylonite at ~300–400 °C in a mid-crustal setting. Shaw and Allen (2007) interpreted the pressure-temperature (PT) conditions of metamorphism during D_2 Paleoproterozoic deformation to be >650–700 °C and 2–5 kbar pressure. Mylonitic pseudotachylytes are found within and adjacent to the D_4 ultramylonites (~300–400 °C; Shaw and Allen, 2007), which indicates at least some, if not all of the pseudotachylyte formed in the middle crust during D_4; this interpretation is discussed in more detail in the field trip stop descriptions. In contrast, application of the O'Hara (2001) geothermometer to pseudotachylytes from the Homestake Creek segment yields ambient host-rock temperatures ranging from 580 to 950 °C (Allen et al., 2002). This range would place the pseudotachylytes in a lower-crustal environment consistent with or earlier than Paleoproterozoic deformation cycles D_1 and D_2. This overestimates the likely depth of generation and is inconsistent with field relations.

Frictional-Plastic Coupling

Field relationships, microstructural observations, and monazite geochronology show that the HSZ became increasingly localized through time, from a broad zone of plastic flow and upright folding at ~1.7 Ga, to a more distributed system of narrow crystal-plastic shear zones and pseudotachylyte-bearing, frictional faults at ~1.4 Ga (Shaw et al., 2001; Shaw and Allen, 2007). An earlier study (Shaw and Allen, 2007) provided an analysis of the evolution of the rheological behavior of the HSZ as conditions of deformation changed through time during protracted lower crustal to mid-crustal exhumation from ~1.7 Ga to ~1.4 Ga, as well as during progressive deformation associated with Mesoproterozoic reactivation of the HSZ at ~1.4 Ga. The Mesoproterozoic deformation cycle produced D_3–D_4 fabrics during exhumation through the middle crust at ~1.4 Ga. The diversity of tectonites developed during this time, ranging from crystal-plastic mylonites and overprinting ultramylonites to brittle-frictional pseudotachylytes, provides an example of the sensitivity of the middle crust to strain-rate variations.

The coeval development of pseudotachylyte and ultramylonite could indicate that: (1) rupture nucleated in the brittle seismogenic zone and propagated downwards into the middle crust, as has been inferred in studies of other pseudotachylytes from sub-seismogenic depths (e.g., Lin et al., 2005; Moecher and Steltenpohl, 2009; Allen and Shaw, 2011); or (2) ultramylonite zones may have been able to transmit and support the

stresses required to elastically load the brittle pseudotachylyte system and generate episodic seismicity (Shaw and Allen, 2007). In this latter model, differential stresses necessary to drive high-strain–rate simple shear in the ultramylonite zone (10^{-10} s^{-1}) are similar to stresses necessary to initiate faulting and drive pseudotachylyte production (300–400 MPa) (Shaw and Allen, 2007). This model implies that brittle and crystal-plastic processes are partitioned into a distinct zone of plastic flow (the Hornsilver–Holy Cross segment) coupled to a dispersed, 3–4-km-wide swath of brittle fault zones (Homestake Creek segment) (Fig. 3). New observations that support this coupling are presented at Stop 2.

Slow or Fast?

The results of recent laboratory experiments by Pec et al. (2012) showing that pseudotachylyte-like material can be generated from preexisting cataclasites during slow creep (~10^{-7} m/s at 300 °C and 500 MPa) raise an interesting question for pseudotachylytes from mid-crustal environments: Could they form as a result of other types of slip such as tectonic tremor, slow and silent earthquakes, or other creep events that are increasingly observed in the instrumented record (e.g., Marone and Richardson, 2010)? The experiments of Pec et al. (2012) were performed on manufactured cataclasites in order to simulate localization on precursory faults filled with grain-size reduced wear products. The amorphous product included thin injection-form veins, flow structures, and embayed lithic clasts; however, it was interpreted to be consistent with nonequilibrium amorphization rather than frictional melting since the experiment did not induce a significant temperature increase.

Field relations and microstructural observations in the HSZ are inconsistent in form with the experimental results, since: (1) many of the Homestake pseudotachylytes appear to be first-generation brittle structures, and (2) those examined in thin section show abundant evidence for formation from a high-temperature melt, such as the growth of dendritic microlites (Fig. 2). We therefore interpret the Homestake pseudotachylytes as products of melting rather than amorphization due to ultracomminution, indicating they serve as records of seismogenic slip.

DESCRIPTION OF FIELD STOPS

Driving instructions: The locations of the field stops are shown in Figure 4. From Denver, proceed west on I-70 to Exit 171 at Minturn and proceed south on U.S. 24E for ~12 mi to Hornsilver Campground in the White River National Forest. Nonstop travel time is ~2 h from the Colorado Convention Center. Stops 1 and 2 are on a prominent bench along the cliffs southeast of the campground. Stops 3–5 can be accessed from White River National Forest Road 703 (Homestake Creek road) ~0.5 mi south of Hornsilver campground on U.S. 24E. Turn right onto Forest Road 703 at the bottom of a prominent switchback on U.S. 24.

Stop 1: Mylonite, Ultramylonite, and Relict Pseudotachylyte at Hornsilver Ridge

The purpose of the first stop is to examine: (1) Paleoproterozoic D_1 and D_2 fabrics recording Paleoproterozoic shortening during continental assembly, and (2) a distinct zone of mylonite and overprinting ultramylonite that document D_3 and D_4 deformation, respectively, in the Hornsilver–Holy Cross segment of the HSZ. Mylonites and ultramylonites are characterized by extensive grain-size reduction, a fine planar foliation, a strong subvertical mineral stretching lineation, and microstructural evidence for lower temperature deformation mechanisms in quartz as compared to S_1 and S_2 domains. At this location, mylonite is more than 50 m thick and is locally overprinted by ultramylonite. The mylonite foliation is oriented 055°, 85°SE on average, and a mineral stretching lineation plunges steeply southwest; shear sense from S-C fabric and asymmetric porphyroclasts shows southeast-side-down kinematics for D_3 mylonites (Shaw et al., 2001; Shaw and Allen, 2007). The overprinting D_4 ultramylonite has a planar foliation oriented 050°, 80°SE on average, and a mineral lineation plunges steeply northeast; shear-sense indicators document southeast-side-up (Shaw and Allen, 2007). Shear sense changes from normal slip in the D_3 mylonites to reverse slip in the D_4 ultramylonites, yet lineations record a consistent component of dextral strike slip for both episodes, consistent with dextral strike slip to oblique slip recorded in pseudotachylytes from the Homestake Creek segment. We have interpreted the persistence of the dextral strike-slip component to be indicative of oblique slip during transpression (Shaw and Allen, 2007). As a result, the reversal in the dip-slip component at this site may represent local reshuffling of subvertical blocks in a dextral transpressional setting.

Pseudotachylyte is associated with brittle microshears in the ultramylonite at this location, and in some thin sections it shows evidence of a ductile overprint (Shaw et al., 2001, 2002). We have also observed thin mm-scale pseudotachylyte with the same mutually overprinting field relations hosted by ultramylonite in outcrops 1 km southwest of Stop 1 on steep, east-facing cliffs above Homestake Creek, and 3 km southwest of the ghost town of Holy Cross City (Fig. 3). Additional details related to Stop 1 are described in Stop 3 of Shaw et al. (2002), and Sites 1–2 of Shaw and Allen (2007).

Stop 2: Pseudotachylyte and Mylonitic Pseudotachylyte at Hornsilver Ridge

A broad, 1–2-km-wide swath of glacial till between the Hornsilver–Holy Cross segment and the Homestake Creek segment to the southwest of this stop conceals a possible connection or gradation between them (Fig. 3). One of the new discoveries presented on this trip is the presence of a northeast-striking zone of pseudotachylyte and mylonitic pseudotachylyte at this locality, which is just 300 m from the previous stop (mylonite, ultramylonite, and relict pseudotachylyte). Numerous subvertical

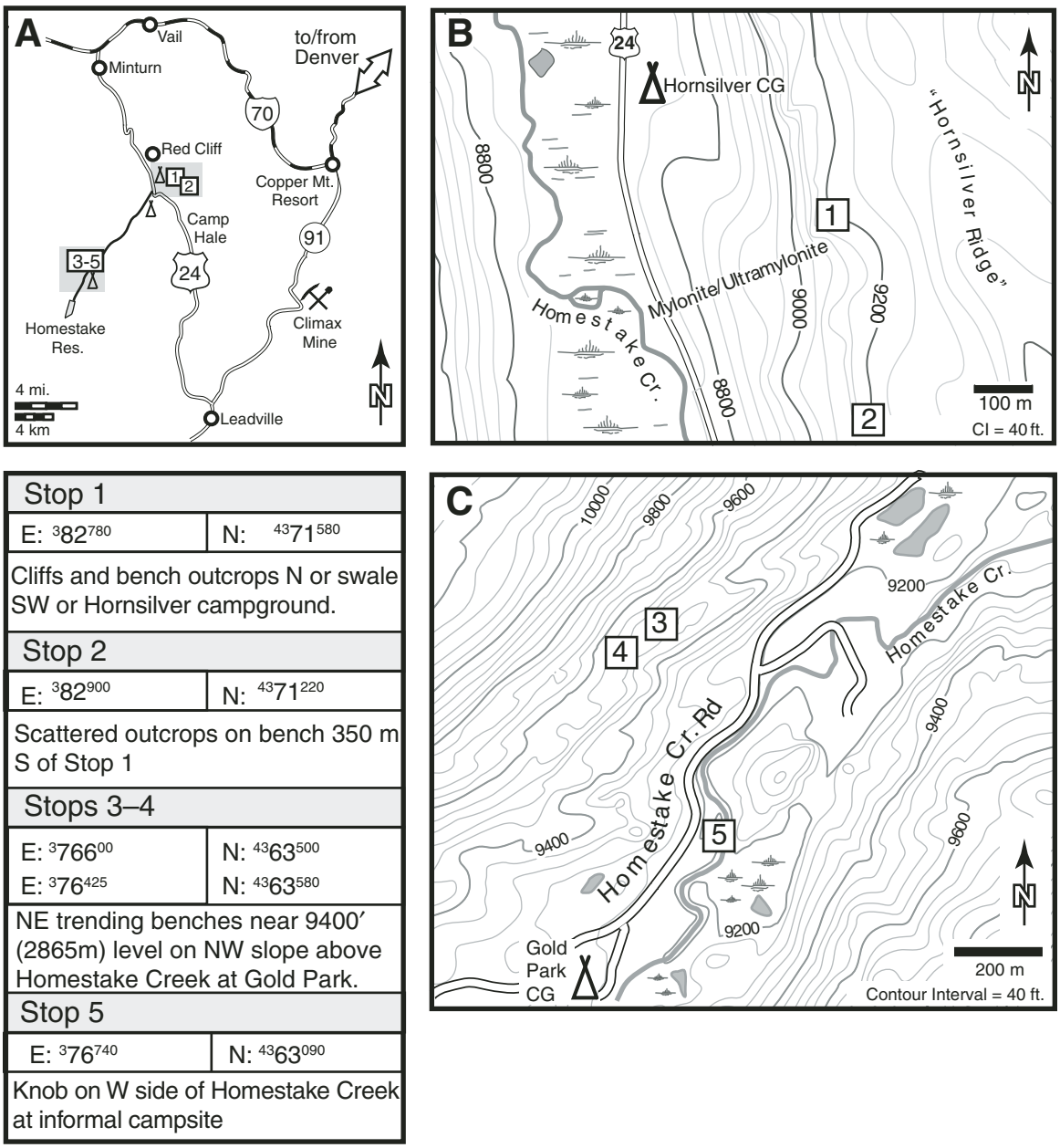

Stop 1	
E: $^{3}82^{780}$	N: $^{43}71^{580}$
Cliffs and bench outcrops N or swale SW or Hornsilver campground.	
Stop 2	
E: $^{3}82^{900}$	N: $^{43}71^{220}$
Scattered outcrops on bench 350 m S of Stop 1	
Stops 3–4	
E: $^{3}766^{00}$ E: $^{3}76^{425}$	N: $^{43}63^{500}$ N: $^{43}63^{580}$
NE trending benches near 9400′ (2865m) level on NW slope above Homestake Creek at Gold Park.	
Stop 5	
E: $^{3}76^{740}$	N: $^{43}63^{090}$
Knob on W side of Homestake Creek at informal campsite	

Figure 4. Location of field trip stops.

pseudotachylyte fault veins with associated injection-vein complexes are present across a 30-m-wide zone. Some of the fault veins exhibit common features of mylonitic and recrystallized pseudotachylyte described elsewhere (e.g., Lin et al., 2005; Lin, 2007; Moecher and Steltenpohl, 2009, 2011; Price et al., 2012; Kirkpatrick and Rowe, 2013), including the presence of elongated, recrystallized quartz ribbons, diminished plastic deformation in protected embayments, and truncated or transposed injection veins (Fig. 5A). Throughout this area, the pseudotachylyte matrix is recrystallized into a fine- to medium-grained mass of new biotite (Figs. 5B–5E) and does not exhibit the aphanitic glassy to cryptocrystalline appearance of veins we will examine in Stops 3–5. Some veins do not show a mylonitic overprint, but the matrix has been recrystallized into coarse biotite (Fig. 5F). The vein fabric is consistent with a static metamorphic overprint (e.g., Kirkpatrick and Rowe, 2013).

Pseudotachylyte fault veins at this locality are typically <1 cm thick, and most are concordant with the foliation of host rocks, which include gneiss and thin, meter-scale mylonite. The fault veins typically strike 045°–055° and dip 80°SE on the southeast side of the fault zone, and 68°–75°NW on the northwest side of the fault zone. The fault zone is localized on the steep limb of a

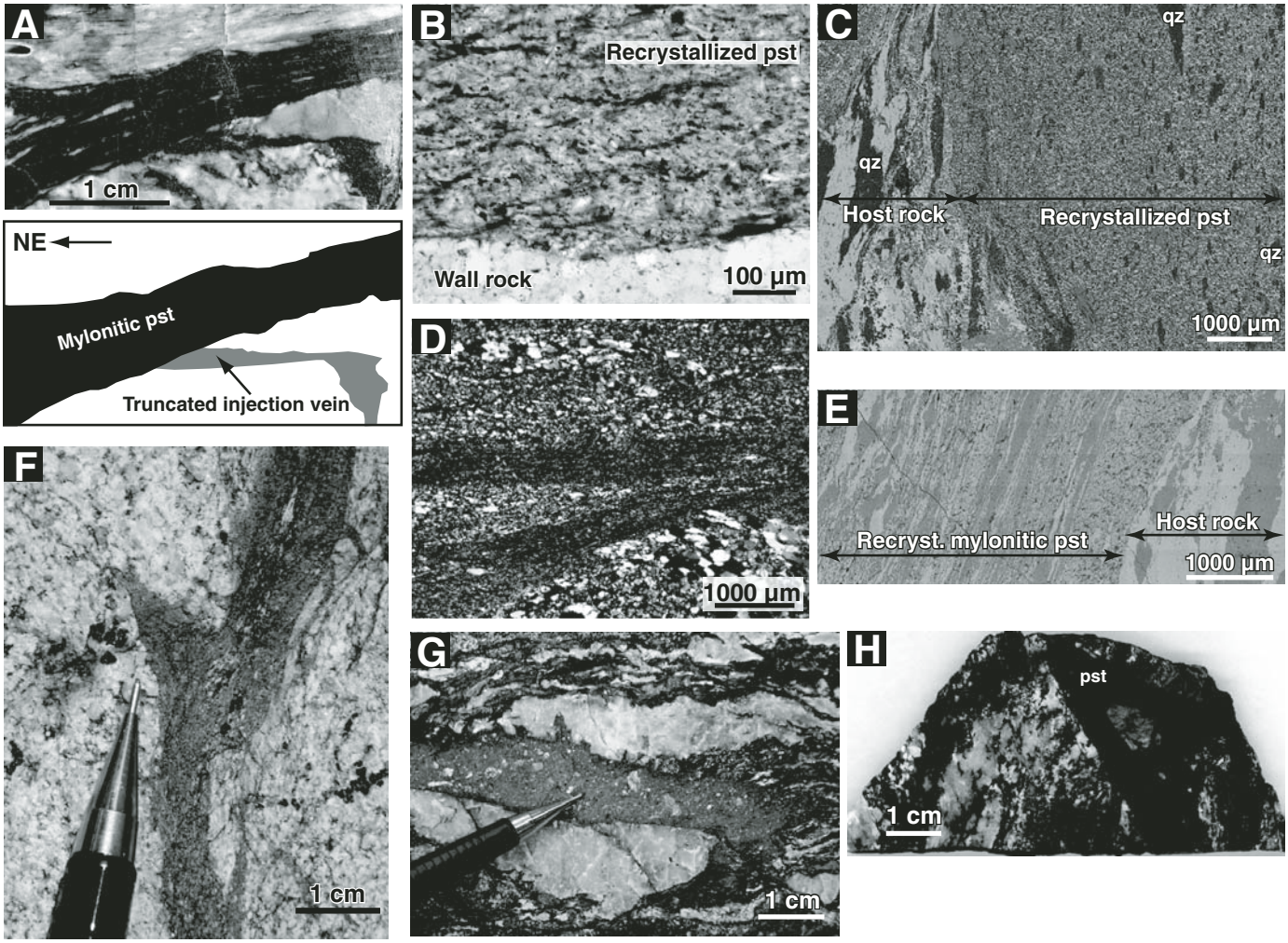

Figure 5. Images of thin sections, polished slabs, and outcrops of representative pseudotachylyte of the Hornsilver–Holy Cross segment. (A) Polished slab and interpretive sketch showing mylonitic pseudotachylyte fault vein with highly elongated quartz ribbons truncating pseudotachylyte injection vein with weaker mylonitic fabric. Horizontal slice through subvertical, N-NE–striking vein. The western block (bottom of photo) is only weakly deformed, which resulted in preservation of the injection vein. The plastically deformed pseudotachylyte marks the boundary of a local shear zone that includes the eastern wall rock (top of photo). (B) Photomicrograph of truncated injection vein shown in (A) above. Note recrystallized biotite with weak preferred fabric. The presence of octahedral magnetite crystals (5–10 µm) suggests the protolith is pseudotachylyte matrix. (C) X-ray compositional image of injection vein showing mixed distribution of K, Al, and Mg (bright areas). (D) Photograph of thin section of mylonitic pseduotachylyte shown in (A). Note recrystallized ribbons of quartz interpreted as plastically deformed and annealed quartz clasts from pseudotachylyte matrix. (E) X-ray compositional image of mylonitic fault vein illustrating strong fabric development. In comparison to (E), fabric in (C) shows quartz (dark) is less elongated and matrix is overprinted by a mass of fine biotite lacking preferential fabric. (F) Outcrop photograph of mylonitic pseudotachylyte fault vein with stretched lithic clasts, truncated injection vein, and rough-weathering appearance as a result of growth of fine-grained biotite in matrix. (G) Fault vein lacking mylonitic overprint but showing rough-weathering matrix of fine-grained biotite. (H) Polished slab cut normal to strike of a fault vein collected from Stop 2; view to SW. The sample shows no plastic overprint, but the matrix is recrystallized into a fine-grained mass of biotite lacking a preferred fabric. Fault vein discordantly cuts foliation and dips NW; field relations suggest it is a reverse fault with top-to-SE displacement. Note: Images shown in (A–E) are from an outcrop of pseudotachylyte 9.5 km SW of Stop 2 (Fig. 3); (F) is from 13 km SW of Stop 2; (G) is from an outcrop 1.5 km SW of Stop 2; and (H) is from Stop 2.

map-scale fold. Immediately southeast of the fault zone, the foliation in the gneiss defines a low-strain, S_1 domain and is oriented 320°, 57°NE. Another narrow northeast-striking zone of subvertical pseudotachylyte and mylonitic pseudotachylyte is similarly localized along the steep limb of a fold 400 m south of Stop 2.

Stop 3: Pseudotachylyte and Deformed Quartz Vein near Gold Park

Stops 3–5 (Fig. 6) show typical field relations in the Homestake Creek segment of the HSZ. This area constitutes the central core of the Homestake shear zone as originally defined by Tweto and Sims (1963). The area encompassing these stops was mapped as an anastomosing system of Precambrian shear zones that "…contain a wide variety of cataclastic rocks: blastomylonites containing large proportions of neomineralized-recrystallized materials, phyllonites, ultramylonites, mylonites, pseudotachylyte, mylonite gneisses, protomylonite, breccias, retrograded rocks, and gouge" (Tweto, 1974). Tweto's pioneering work generated a 1:24,000 scale, 15 min quadrangle with a remarkable level of detail. The map utilized the older fault-rock terminology of Higgins (1971) and incorporated all of the fault rocks into a single map unit labeled as "cataclastic gneiss." Tweto's mapping shows most of the individual shear zones to be 10–30 m wide, and he describes them as "…intruded by pegmatite, unclassified granite (ug), hornblendite, hornblende diorite, and metalamprophyre." Building upon this work, we have isolated many of the fault rocks into separate mappable units (Fig. 3). This effectively redefines the HSZ as a distributed system of D_3–D_4 tectonites (pseudotachylyte, mylonite, and ultramylonite) that overprint D_1–D_2 fabrics and folds. Most of the braided cataclastic gneisses of Tweto (1974) are interpreted as locally mylonitic high-strain zones that wrap around lower-strain lozenges (Shaw and Allen, 2007). In this interpretation, the high-strain zones originated as D_2 domains where D_1 foliation was transposed into a subvertical, northeast-striking composite foliation along the limbs of subvertical folds. Most of the high-strain zones consist of strongly transposed, 055°–060° striking fabrics, and interlayers of semi-pelitic biotite gneiss and pelitic schist (Fig. 2A). Locally, the high-strain zones are mylonitic and probably related to D_2 transposition (Shaw and Allen, 2007); however, we have also recognized some mylonitic fabrics that appear to be younger and possibly related to D_3 or D_4 deformation (see below). In general these younger fabrics are restricted to fairly narrow shear zones that can be recognized by very fine-grained "cherty" textures and well-defined strain gradients marking their margins.

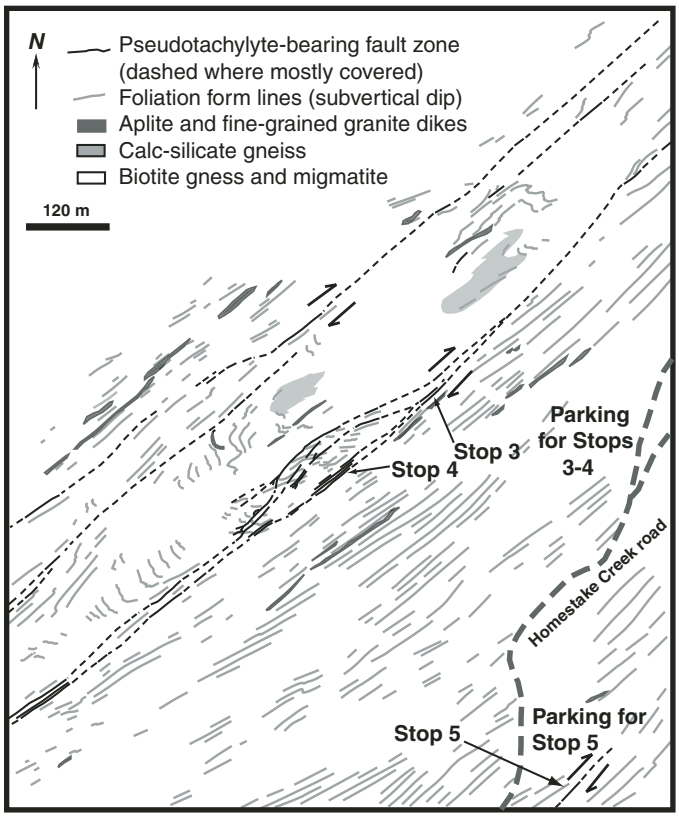

Figure 6. Geologic map of the Gold Park vicinity showing the locations of Stops 3–5. In this area, pseudotachylyte-bearing fault zones each consist of several to several dozen fault veins with associated injection veins and pseudotachylyte-filled damage zones (see Fig. 7 for outcrop-scale distribution). Fault zones follow a transposed, NE-striking foliation and are separated from each other by a lower-strain region of oblique foliation (Allen, 2005). Where crosscutting relations between pseudotachylyte fault veins and host rock markers can be observed, fault veins dominantly show strike-slip to oblique-slip, dextral kinematics in this area.

Along the Homestake Creek segment of the HSZ, many of the northeast-striking, high-strain zones served to localize earthquake rupture propagation, as evidenced by development and preservation of the extensive pseudotachylyte system shown in Figure 3. Lower-strain domains preserving D_1 fabrics are present between the pseudotachylyte-bearing fault zones (Fig. 2B). These lower-strain domains are characterized by outcrop-scale z-folds and a foliation that bends from 055° to 060° to a 090°–110° orientation; they seldom host pseudotachylyte. The folding is often well defined by the interlayered pelitic schist unit. Additional details related to this site are described in Stop 2B of Allen et al. (2002) and Site 3 of Shaw and Allen (2007).

This stop highlights a particularly informative outcrop where a quartz vein is offset by multiple pseudotachylyte-bearing faults and mylonitic shear zones. The quartz vein exhibits microstructures including amoeboid grain boundaries and "chess board" extinction consistent with high-temperature deformation in the beta-quartz stability field (>573 °C). Abundant planar arrays of fluid inclusions may indicate an early generation of "healed" fractures. A range of crystal-plastic, cataclastic and brittle shears, microfaults, and fractures cuts across older microstructures. The abundance of these younger features increases toward the pseudotachylyte zones with major sets coinciding with Riedel orientations (R, R′, and P). Possible crystal-plastic microshears occur adjacent to the pseudotachylyte zones (e.g., Bestmann et

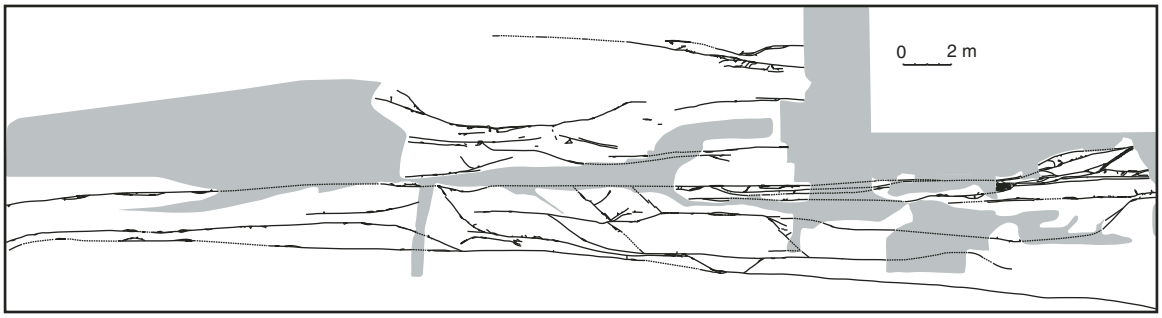

Figure 7. Outcrop map of pseudotachylytes from Stop 4 (modified from Shaw and Allen, 2007). The along-strike continuity of pseudotachylyte and the lack of significant cataclasite-bearing faults indicate that fault-zone development was dominated by processes related to frictional melting (and thus earthquake seismicity). Gray areas show distribution of cover.

al., 2004, 2012; Pennacchioni, 2005). In one sample, the wall of the pseudotachylyte fault consists of a microbreccia that is partially dismembered and crosscut by injection veins. We suggest that microstructures preserved in this quartz vein represent a sequence of pre-, syn- and (perhaps) postrupture deformation of the wall rock of the this strand of the pseudotachylyte fault zone.

Stop 4: Pseudotachylyte and Low-Strain Domain near Gold Park

At this stop, multiple generations of pseudotachylyte are preserved across a 12-m-wide fault zone concordant to foliation (Fig. 7). Some of the fault veins include transfer faults between paired faults, similar to those described in other systems (e.g., Swanson, 2006). In contrast to the previous stop, the host rock is dominantly pelitic gneiss and schist. As a result, this outcrop shows complex injection-vein networks and local phyllosilicate cataclasites that constitute the damage zone of adjacent fault veins (Fig. 8). Outcrops 50 m N-NE of Stop 4 show excellent examples of lower-strain S_1 fabrics in the supracrustal gneisses. Additional details related to this field site are described in Stop 2C of Allen et al. (2002) and Site 3 of Shaw and Allen (2007).

Stop 5 (Optional): Pseudotachylyte near the Northeastern End of a Fault Zone

At this stop, multiple generations of pseudotachylyte are preserved in a relatively narrow fault zone (~3–4 m wide) locally hosted by mylonitic gneiss. It is unclear whether this is an older Paleoproterozoic mylonite (perhaps related to D_2) or a product of Mesoproterozoic reactivation as inferred for the thin mylonite band at Stop 3. In thin section, some pseudotachylytes show elongated lithic clasts, suggesting the possibility of a localized plastic overprint. The overall width of the fault zone and the width of individual fault veins are thin as compared to Stops 3 and 4. This reflects a broader observation that fault zones thin and pseudotachylytes become less abundant from southwest to northeast along individual fault zones in the Homestake Creek segment (Allen, 2005).

SUMMARY AND DISCUSSION

As presently mapped, the HSZ features a 25-km-long system of pseudotachylyte, recrystallized and mylonitic pseudotachylyte, mylonite, and ultramylonite. The shear zone developed as a high-temperature structure during Paleoproterozoic continental assembly at ~1.7 Ga as recorded by deformation cycles D_1–D_2. It was reactivated as a Mesoproterozoic, subvertical transpressional system at ~1.4 Ga under lower-temperature conditions in a mid-crustal, intracontinental setting. This latter deformation cycle (D_3–D_4) was at least in part seismogenic, as recorded by brittle-plastic pseudotachylytes in D_4 ultramylonite (Shaw et al., 2001, 2002). The HSZ shows a progressive, strike-perpendicular strain gradient from northwest to southeast, from: (1) ultramylonites and recrystallized mylonitic pseudotachylyte on the northwest (the Hornsilver–Holy Cross segment), to (2) more pristine pseudotachylytes on the southeast (the Homestake Creek and Savage segments). The tectonites in all of these segments are systematically localized into numerous meter- to decameter-scale fault zones dispersed across the width of the

Figure 8. Polished slab, photomicrographs, and X-ray compositional maps from a representative pelitic gneiss/schist sampled from vicinity of Stop 4 (sample 206-93; whole-rock chemical data for bulk pseudotachylyte and host rock shown in columns 13 and 14, Table 2). (A) Polished slab and interpretative illustration showing multiple generations of pseudotachylyte (black in illustration) and phyllosilicate-rich cataclasite (brown in illustration) in a biotite-rich host. Thick pseudotachylyte (pst) vein on right includes gray-weathering matrix band. Sample cut normal to 055° foliation and fault vein strike; view to NE. (B) X-ray compositional maps (K, Fe, and Si) showing mesoscopic textural and chemical variations between host rock and pst (19.4 cm^2 area analyzed by μXRF [micro–X-ray fluorescence]). (C) Photomicrograph (PPL) from thin section of thick pst vein shown in (A) illustrating diffuse contact between gray-weathering matrix and black opaque matrix indicating they formed as single event rather than overprinting involving two generations of pst (gray matrix is light brown under PPL). (D) Photomicrograph (PPL) of short injection vein branching from 1-cm-thick pst fault vein shown on left side of (A). Brown-colored rim is inferred to be a quenched melt margin at the intrusive pst contact.

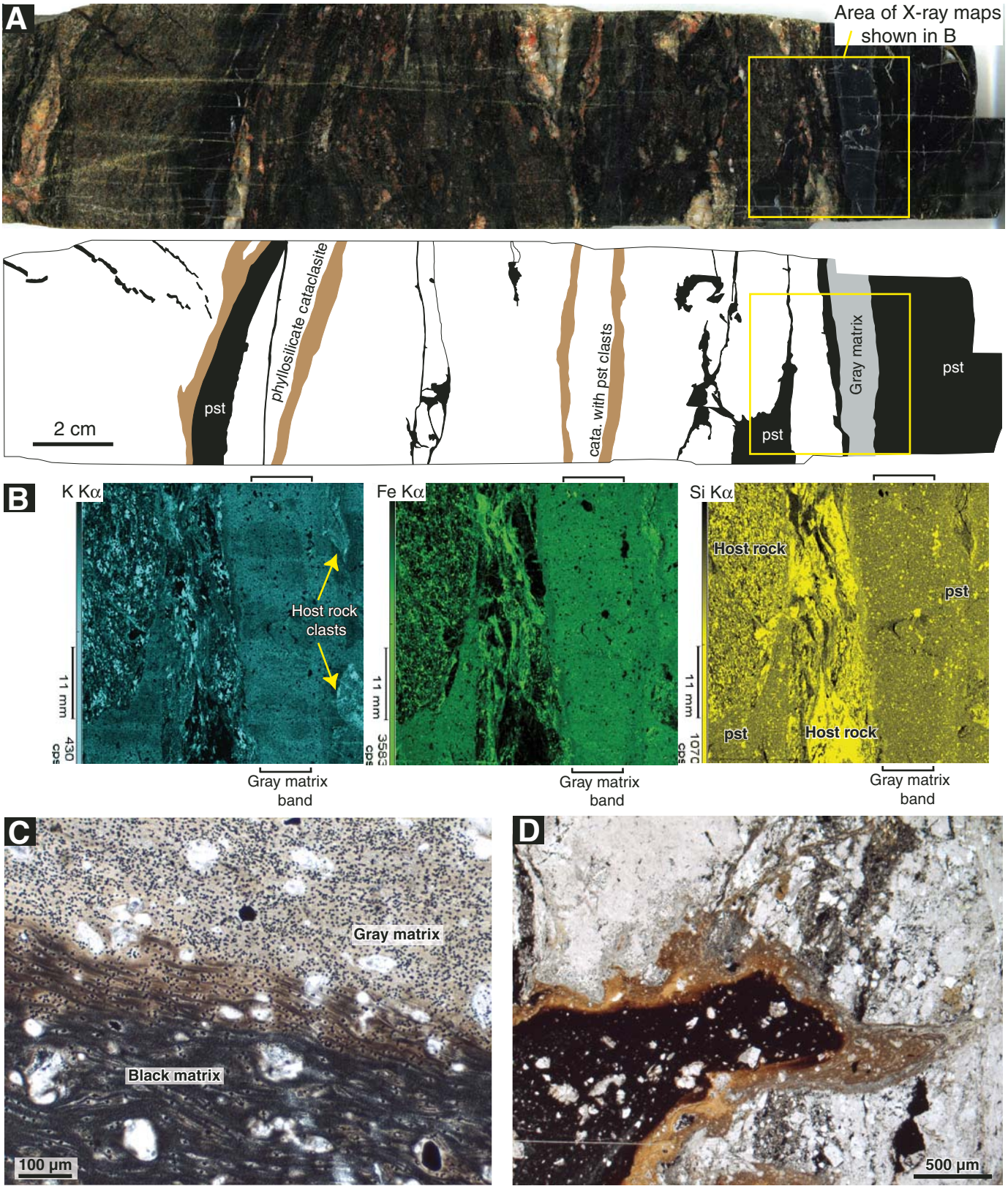
A
Area of X-ray maps shown in B
pst
phyllosilicate cataclasite
cata. with pst clasts
Gray matrix
pst
pst
2 cm
B
K Kα
Host rock clasts
11 mm
430 cps
Gray matrix band
Fe Kα
11 mm
3583 cps
Gray matrix band
Si Kα
Host rock
pst
11 mm
1070 cps
pst
Host rock
Gray matrix band
C
Gray matrix
Black matrix
100 µm
D
500 µm

shear zone. As a result, the HSZ uniquely preserves exhumed details of earthquake rupture at the fault-system scale. Two aspects of this distribution are briefly discussed: (1) geologic controls on the distribution of mylonite series rocks and seismogenic fault zones, and (2) the nature of the systematic strain gradient and implications for heterogeneity and "roughness" near the base of the seismogenic zone.

Geologic Controls on the Distribution of Mylonite and Pseudotachylyte

The seismogenic fault zones in the Homestake Creek segment are all concordant with high-strain zones consisting of subvertical, highly transposed foliation interpreted to have formed as an early D_2 event. Lower-strain (S_1) domains that preserve mesoscopic z-folds and oblique, E-W to NW-SE foliation trends lie between most of the fault zones (Fig. 6). Similarly, the mylonite and ultramylonite of the Hornsilver–Holy Cross segment comprise a zone of NE-striking foliation. The map-scale distribution of the pseudotachylyte-bearing fault zones is therefore strongly controlled by a preexisting Paleoproterozoic anisotropy in the supracrustal gneisses south and southeast of the ~1.7 Ga Cross Creek granite (Fig. 3).

A prominent feature of the HSZ is the strike-perpendicular asymmetry of the system, with mylonite series rocks on the NW and pseudotachylytes restricted to the SE. Preexisting structure may also control this pattern, since gneisses north and northwest of the Hornsilver–Holy Cross segment generally strike E-W to SE-NW, and the lithology is dominated by rocks with >50%–60% migmatitic leucosomes (Fig. 9). Tweto (1974) and Tweto and Lovering (1977) noted that the biotite gneisses become much more migmatitic (and were termed "structurally disorganized") from south to north across the HSZ; they attributed this trend to increasing proximity to the ~1.7 Ga Cross Creek batholith north of the HSZ. The map pattern in Figure 3 suggests that the Cross Creek batholith, rimmed by migmatite, formed a backstop during Mesoproterozoic transpressional reactivation of the HSZ. In this speculative model, mylonite first localized along a NE-striking D_2 domain near the outer margin of the migmatite rim during the D_3 deformation cycle. This fabric was then overprinted during generation of the D_4 ultramylonite and pseudotachylytes that comprise the Hornsilver–Holy Cross segment.

Figure 9. Outcrop of migmatite 0.5 km NW of the Hornsilver–Holy Cross ultramylonite. Compare extensive leucosome development with image of gneiss from high-strain zone in Figure 2A.

Implications for Roughness near the Base of the Seismogenic Zone

The systematic strain gradient suggests development of the Hornsilver–Holy Cross segment was essentially coeval with development of pseudotachylytes comprising the Homestake Creek segment (and the Savage segment to the southwest). The model of Shaw and Allen (2007) proposed that seismicity could result from intermittent release of stress that accumulated in country rocks during progressive displacement associated with the Hornsilver–Holy Cross ultramylonite. This interpretation implies that pseudotachylyte in the Homestake Creek segment was generated within the middle crust rather than forming as a result of down-dip rupture propagation from higher in the seismogenic zone. The Shaw and Allen (2007) model is consistent with: (1) a lack of meteoric fluids in the pseudotachylyte (Moecher and Sharp, 2004), (2) the lack of a brittle fault core composed of gouge or cataclasite that would be expected if the HSZ had been progressively exhumed during deformation associated with pseudotachylyte development, and (3) the relatively small number of fault veins noted in each fault zone (several to several dozen) suggesting the development of pseudotachylyte was relatively uncommon. The model also implies that the pseudotachylyte need not be vertically linked to brittle faults in the overlying seismogenic zone.

If brittle and plastic faults were active at the same crustal level, it implies that the middle crust can exhibit lateral "roughness" (as proposed by Sibson, 1984), where variations in temperature, strain rate, and lithology near the base of the seismogenic zone lead to variations in shear resistance and rheology at the kilometric scale. This can result in lateral variations in depth to the brittle-plastic transition. On the basis of microstructural observations, Trepmann and Stockhert (2003) considered this notion in more detail and inferred that major earthquakes could reshape the distribution of stress and cause a temporary deepening of the brittle-plastic transition. As an extension of that study to an active fault zone, Rolandone et al. (2004) examined the time-dependent depth distribution of aftershock seismicity at the fault-segment scale for the 1992 M 7.3 Landers earthquake. They found that the brittle-plastic transition temporarily deepened by 2–3 km after that event in response to a transient, strain-rate–driven increase in postseismic stresses, which implies a mechanical control on the depth to the base of the seismogenic zone following large earthquakes. This allows brittle rupture in the form

of aftershocks to occur at depths below the long-term base of the seismogenic zone. As an application of this concept to the HSZ, the Hornsilver–Holy Cross segment may have developed at a strain rate and temperature suitable for crystal-plastic deformation, whereas rocks up to 4 km to the southeast may have been somewhat cooler and/or weaker, favoring brittle seismogenic rupture. The pronounced D_2 mechanical anisotropy along the Homestake Creek and Savage segments provided relatively weak zones susceptible to failure at lower shear stresses than the strongly migmatitic rocks northwest of the Hornsilver–Holy Cross segment. In fact, Tweto (1974) originally mapped a strong swarm of braided "cataclastic gneisses" along the south-facing slopes of the Homestake Creek valley and thus recorded this anisotropy in his mapping. Considering the results of Rolandone et al. (2004), it is possible that at least some of the Homestake pseudotachylytes might reflect deep aftershocks in the middle crust following a larger earthquake higher in the overlying seismogenic zone (which is not preserved in the rock record in this fault system). A temporary deepening of the brittle-plastic transition following such an event could lead to failure and generation of frictional melts along northeast-striking, transposed D_2 domains.

As an alternative interpretation, the pseudotachylyte in the Hornsilver–Holy Cross segment and the Homestake Creek and Savage segments formed at different times, at different crustal levels, or both. Presumably, the Hornsilver–Holy Cross segment with mylonite and mylonitic pseudotachylyte might be considered older and deeper and the brittle Homestake Creek and Savage segments might be considered younger and shallower. If these formed at different times and different structural levels, however, it does not explain why pristine, undeformed pseudotachylyte did not overprint and exploit the ultramylonite and adjacent rocks in the Hornsilver–Holy Cross segment, which shares the same anisotropic fabric as the Homestake Creek segment. The Homestake Creek segment would have had to fortuitously develop adjacent to the Hornsilver–Holy Cross segment at a later time and not overprint it, which seems unlikely.

By analogy, the distribution of pseudotachylytes from the HSZ may have implications for the deep structure of seismically active fault zones. Whereas many active strike-slip faults such as the southern Alpine fault and the San Andreas fault are frictionally weak and accommodate large displacements localized into a narrow (m-scale) fault core (e.g., Chester et al., 1993; Barth et al., 2013), the HSZ shows that seismicity was delocalized and dispersed across discrete, relatively narrow fault zones spanning a width of 3–4 km. In contrast to weak faults, frictionally strong seismogenic faults, such as the exhumed Gole Larghe fault in the Italian Alps, show low displacement/fault thickness ratios and are dominated by hardening processes such as mineral cementation in cataclasites and the formation of pseudotachylytes (Di Toro and Pennacchioni, 2005). We suggest that the HSZ is an additional example of a strong-type seismogenic fault, following the definition of Di Toro and Pennacchioni (2005). Active fault zones that overprint heterogeneous fabrics in basement metamorphic rocks at or near the base of the seismogenic zone may show similarly dispersed systems of seismicity, although it may be challenging to conclusively image such structures without dense arrays.

ACKNOWLEDGMENTS

Research supported by the National Science Foundation (EAR-0635894 and EAR-0635920), the Allie Irene Strasko Research Trust Fund at Concord University, and the West Virginia Higher Education Policy Commission Division of Science and Research. Numerous undergraduate students provided valuable field and laboratory assistance, including Albert Barbery, Christina Facemyer, Sean Gillian, Billy Lacek, Gary Thompson, Ian Ware, and participants in the 2013 Concord geology field camp. Reviews by Phil Resor and Mark Swanson improved the content of the manuscript.

REFERENCES CITED

Allen, J.L., 2004, Timing, style, and significance of Cambrian through Laramide brittle reactivation along the Proterozoic Homestake shear zone, Colorado mineral belt: Rocky Mountain Geology, v. 39, no. 2, p. 65–84, doi:10.2113/39.2.65.

Allen, J.L., 2005, A multi-kilometer pseudotachylyte system as an exhumed record of earthquake rupture geometry at hypocentral depths (Colorado, USA): Tectonophysics, v. 402, no. 1–4, p. 37–54, doi:10.1016/j.tecto.2004.10.017.

Allen, J.L., and Shaw, C.A., 2008, Proterozoic geology and Phanerozoic reactivation of the newly recognized Grizzly Creek shear zone, Glenwood Canyon, Colorado, *in* Raynolds, R.G., ed., Roaming the Rocky Mountains and Environs: Geological Field Trips: Geological Society of America Field Guide 10, p. 45–61, doi:10.1130/2007.fld010(03).

Allen, J.L., and Shaw, C.A., 2011, Seismogenic structure of a crystalline thrust fault: Fabric anisotropy and coeval pseudotachylyte-mylonitic pseudotachylyte in the Grizzly Creek shear zone, Colorado, *in* Fagereng, Å., Toy, V.G., and Rowland, J., eds., Geology of the Earthquake Source: A Volume in Honour of Rick Sibson: Geological Society of London, Special Publication 359, p. 135–151.

Allen, J.L., O'Hara, K.D., and Moecher, D.P., 2002, Structural geometry and thermal history of pseudotachylyte from the Homestake shear zone, Sawatch Range, Colorado, *in* Lageson, D., ed., Science at the Highest Level: Geological Society of America Field Guide 3, p. 17–32, doi:10.1130/0-8137-0003-5.17.

Amato, J.M., Boullion, A.O., Serna, A.M., Sanders, A.E., Farmer, G.L., Gehrels, G.E., and Wooden, J.L., 2008, Evolution of the Mazatzal province and the timing of the Mazatzal orogeny: Insights from U-Pb geochronology and geochemistry of igneous and metasedimentary rocks in southern New Mexico: Geological Society of America Bulletin, v. 120, p. 328–346, doi:10.1130/B26200.1.

Anderson, J.L., 1983, Proterozoic anorogenic granite plutonism of North America, *in* Medaris, L.G., Jr., Byers, C.W., Mickelson, D.M., and Shanks, W.C., eds., Proterozoic Geology: Selected papers from an international Proterozoic symposium: Geological Society of America Memoir 161, p. 133–154, doi:10.1130/MEM161-p133.

Barnhart, K.R., Walsh, P.J., Hollister, L.S., Daniel, C.G., and Andronicos, C.L., 2012, Decompression during the late Proterozoic Al_2SiO_5 triple-point metamorphism at Cerro Colorado, New Mexico: The Journal of Geology, v. 120, p. 385–404, doi:10.1086/665793.

Barth, N.C., Boulton, C., Carpenter, B.M., Batt, G.E., and Toy, V.G., 2013, Slip localization on the southern Alpine Fault, New Zealand: Tectonics, v. 32, p. 1–21, doi:10.1002/tect.20041.

Berlenbach, J.W., and Roering, C., 1992, Sheath-fold-like structures in pseudotachylytes: Journal of Structural Geology, v. 14, no. 7, p. 847–856, doi:10.1016/0191-8141(92)90045-X.

Bestmann, M., Prior, D., and Veltkamp, K.T.A., 2004, Development of single-crystal sigma-shaped quartz porphyroclasts by dissolution-precipitation creep in a calcite marble shear zone: Journal of Structural Geology, v. 26, p. 869–883, doi:10.1016/j.jsg.2003.10.003.

Bestmann, M., Pennacchioni, G., Nielsen, S., Göken, M., and de Wall, H., 2012, Deformation and ultrafine dynamic recrystallization of quartz in pseudotachylyte-bearing brittle faults: A matter of a few seconds: Journal of Structural Geology, v. 38, p. 21–38, doi:10.1016/j.jsg.2011.10.001.

Bickford, M.E., 1988, The accretion of Proterozoic crust in Colorado: Igneous, sedimentary, deformational, and metamorphic history, *in* Ernst, W.G., ed., Metamorphism and Crustal Evolution of the Western United States: Englewood Cliffs, Prentice Hall, p. 411–429.

Bickford, M.E., Mueller, P.A., Kamenov, G.D., and Hill, B.M., 2008, Crustal evolution of southern Laurentia during the Paleoproterozoic: Insights from zircon Hf isotopic studies of ca. 1.75 Ga rocks in central Colorado: Geology, v. 36, p. 555–558, doi:10.1130/G24700A.1.

Chester, F.M., Evans, J.P., and Biegel, R.L., 1993, Internal structure and weakening mechanism of the San Andreas Fault: Journal of Geophysical Research, v. 98, p. 771–786, doi:10.1029/92JB01866.

Di Toro, G., and Pennacchioni, G., 2005, Fault plane processes and mesoscopic structure of a strong-type seismogenic fault in tonalites (Adamello batholith, Southern Alps): Tectonophysics, v. 402, no. 1–4, p. 55–80, doi:10.1016/j.tecto.2004.12.036.

Di Toro, G., Hirose, S., Nielsen, S., Pennacchioni, G., and Shimamoto, T., 2006, Natural and experimental evidence of melt lubrication of faults during earthquakes: Science, v. 311, p. 647–649, doi:10.1126/science.1121012.

Di Toro, G., Pennacchioni, G., and Nielsen, S., 2009, Pseudotachylytes and earthquake source mechanics, *in*, Fukuyama, E., ed., Fault-Zone Properties and Earthquake Rupture Dynamics: Academic Press, p. 87–133.

Di Toro, G., Han, R., Hirose, T., De Paola, N., Nielsen, S., Mizoguchi, K., Ferri, F., Cocco, M., and Shimamoto, T., 2011, Fault lubrication during earthquakes: Nature, v. 471, p. 494–498, doi:10.1038/nature09838.

Fabbri, O., Lin, A., and Tokushige, H., 2000, Coeval formation of cataclasite and pseudotachylyte in a Miocene forearc granodiorite, southern Kyushu, Japan: Journal of Structural Geology, v. 22, no. 8, p. 1015–1025, doi:10.1016/S0191-8141(00)00021-3.

Fiske, P.S., Nellis, W.J., Lipp, M., Lorenzana, H., Kikuchi, M., and Syono, Y., 1995, Pseudotachylites generated in shock experiments: Implications for impact cratering products processes: Science, v. 270, no. 5234, p. 281–283, doi:10.1126/science.270.5234.281.

Griffith, W.A., Di Toro, G., Pennacchioni, G., and Pollard, D.D., 2008, Thin pseudotachylytes in faults of the Mt. Abbot Quadrangle, Sierra Nevada: Physical constraints for small seismic slip events: Journal of Structural Geology, v. 30, p. 1086–1094, doi:10.1016/j.jsg.2008.05.003.

Grunewald, U.R., Sparks, S.J., Kearns, S., and Komorowski, J.C., 2000, Friction marks on blocks from pyroclastic flows at the Soufriere Hills volcano, Montserrat: Implication for flow mechanisms: Geology, v. 28, p. 827–830, doi:10.1130/0091-7613(2000)28<827:FMOBFP>2.0.CO;2.

Higgins, M.W., 1971, Cataclastic Rocks: U.S. Geological Survey Professional Paper 687, 97 p.

Hoffman, P.F., 1989, Precambrian geology and tectonic history of North America, *in* Bally, A.W., and Palmer, A.R., eds., The Geology of North America—An Overview: The Geology of North America: Boulder, Geological Society of America, v. A, p. 447–512.

Jones, J.V., III, Connelly, J.N., Karlstrom, K.E., Williams, M.L., and Doe, M.F., 2009, Age, provenance, and tectonic setting of Paleoproterozoic quartzite successions in the southwestern United States: Geological Society of America Bulletin, v. 121, p. 247–264.

Karlstrom, K.E., and Bowring, S.A., 1988, Early Proterozoic assembly of tectonostratigraphic terranes in southwestern North America: The Journal of Geology, v. 96, p. 561–576, doi:10.1086/629252.

Kenkmann, T., Hornemann, U., and Stöffler, D., 2000, Experimental generation of shock-induced pseudotachylites along lithological interfaces: Meteoritics & Planetary Science, v. 35, no. 6, p. 1275–1290, doi:10.1111/j.1945-5100.2000.tb01516.x.

Kirby, E., Karlstrom, K.E., Andronicos, C.L., and Dallmeyer, R.D., 1995, Tectonic setting of the Sandia Pluton: An orogenic 1.4 Ga granite in New Mexico: Tectonics, v. 14, p. 185–201, doi:10.1029/94TC02699.

Kirkpatrick, J.D., and Rowe, C.D., 2013, Disappearing ink: How pseudotachylytes are lost from the rock record: Journal of Structural Geology, v. 52, p. 183–198, doi:10.1016/j.jsg.2013.03.003.

Lee, P.E., Jessup, M.J., Shaw, C.A., Hicks, G.L., and Allen, J.L., 2012, Strain partitioning in the mid-crust of a transpressional shear zone system: Insights from the Homestake and Slide Lake shear zones, central Colorado: Journal of Structural Geology, v. 39, p. 237–252, doi:10.1016/j.jsg.2012.02.006.

Lin, A., 2007, Fossil Earthquakes: The Formation and Preservation of Pseudotachylytes: Berlin, Springer, 348 p.

Lin, A., and Shimamoto, T., 1998, Selective melting processes as inferred from experimentally generated pseudotachylytes: Journal of Asian Earth Sciences, v. 16, p. 533–545, doi:10.1016/S0743-9547(98)00040-3.

Lin, A., Chen, A., Liau, C.-F., Lee, C.-T., Lin, C.-C., Lin, P.-S., Wen, S.-C., and Ouchi, T., 2001, Frictional fusion due to coseismic landsliding during the 1999 Chi-Chi (Taiwan) ML 7.3 Earthquake: Geophysical Research Letters, v. 28, no. 20, p. 4011–4014, doi:10.1029/2001GL013253.

Lin, A., Maruyama, T., Aaron, S., Michibayashi, K., Camacho, A., and Kano, K., 2005, Propagation of seismic slip from brittle to ductile crust: Evidence from pseudotachylyte of the Woodroffe thrust, central Australia: Tectonophysics, v. 402, p. 21–35, doi:10.1016/j.tecto.2004.10.016.

Maddock, R.H., 1992, Effects of lithology, cataclasis and melting on the composition of fault-generated pseudotachylytes in Lewisian gneiss, Scotland: Tectonophysics, v. 204, p. 261–278, doi:10.1016/0040-1951(92)90311-S.

Magloughlin, J.F., 1992, Microstructural and chemical changes associated with cataclasis and frictional melting at shallow crustal levels: The cataclasite-pseudotachylyte connection: Tectonophysics, v. 204, p. 243–260, doi:10.1016/0040-1951(92)90310-3.

Marone, C., and Richardson, E., 2010, Learning to read fault-slip behavior from fault-zone structure: Geology, v. 38, no. 8, p. 767–768, doi:10:1130/focus082010.1.

Masch, L., Wenk, H.R., and Preuss, E., 1985, Electron microscopy study of hyalomylonites—Evidence for frictional melting in landslides: Tectonophysics, v. 115, no. 1–2, p. 131–160, doi:10.1016/0040-1951(85)90103-9.

McCoy, A.M., Karlstrom, K.E., and Shaw, C.A., 2005, The Proterozoic ancestry of the Colorado mineral belt: 1.4 Ga shear zone system in central Colorado, *in* Karlstrom, K.E., and Keller, G.R., eds., The Rocky Mountain Region—An Evolving Lithosphere: Tectonics, Geochemistry, and Geophysics: American Geophysical Union Geophysical Monograph Series 154, p. 71–90.

Melosh, H.J., 2005, The mechanics of pseudotachylyte formation in impact events, *in* Koeberl, C., and Henkel, H., eds., Impact Tectonics: Springer, p. 55–80.

Moecher, D.P., and Brearley, A.J., 2004, Mineralogy and petrology of a mullite-bearing pseudotachylyte: Constraints on the temperature of coseismic frictional fusion: The American Mineralogist, v. 89, p. 1486–1495.

Moecher, D.P., and Sharp, Z.D., 2004, Stable isotope and chemical systematics of pseudotachylyte and wall rock, Homestake shear zone, Colorado, USA: Meteoric fluid or rock-buffered conditions during coseismic fusion?: Journal of Geophysical Research, v. 109, p. B12206, doi:10.1029/2004JB003045.

Moecher, D.P., and Steltenpohl, M.G., 2009, Direct calculation of rupture depth for an exhumed paleoseismogenic fault from mylonitic pseudotachylyte: Geology, v. 37, p. 999–1002, doi:10.1130/G30166A.1.

Moecher, D.P., and Steltenpohl, M.G., 2011, Petrological evidence for coseismic slip in extending middle-lower continental crust: Heir's zone of pseudotachylyte, north Norway, *in* Fagereng, Å., Toy, V.G., and Rowland, J., eds., Geology of the Earthquake Source: A Volume in Honour of Rick Sibson: Geological Society of London, Special Publication 359, p. 169–186.

Niemeijer, A., Di Toro, G., Griffith, W.A., Bistacchi, A., Smith, S.A.F., and Nielsen, S., 2012, Inferring earthquake physics and chemistry using an integrated field and laboratory approach: Journal of Structural Geology, v. 39, p. 2–36, doi:10.1016/j.jsg.2012.02.018.

Nyman, M.W., Karlstrom, K.E., Kirby, E., and Graubard, C.M., 1994, Mesoproterozoic contractional orogeny in western North America: Evidence from ca. 1.4 Ga plutons: Geology, v. 22, p. 901–904, doi:10.1130/0091-7613(1994)022<0901:MCOIWN>2.3.CO;2.

O'Hara, K.D., 2001, A pseudotachylyte geothermometer: Journal of Structural Geology, v. 23, p. 1345–1357, doi:10.1016/S0191-8141(01)00008-6.

O'Hara, K.D., and Huggins, F.E., 2005, A Mössbauer study of pseudotachylytes: Redox conditions during seismogenic faulting: Contributions to Mineralogy and Petrology, v. 148, p. 602–614, doi:10.1007/s00410-004-0622-y.

O'Hara, K.D., and Sharp, Z.D., 2001, Chemical and oxygen isotope composition of natural and artificial pseudotachylyte: Role of water during frictional fusion: Earth and Planetary Science Letters, v. 184, p. 393–406, doi:10.1016/S0012-821X(00)00331-9.

Pearson, R.C., Hedge, C.E., Thomas, H.H., and Stearn, T.W., 1966, Geochronology of the St. Kevin Granite and neighboring Precambrian rocks,

northern Sawatch Range, Colorado: Geological Society of America Bulletin, v. 77, p. 1109–1120, doi:10.1130/0016-7606(1966)77[1109:GOTSKG]2.0.CO;2.

Pec, M., Stünitz, H., Heilbronner, R., Dryry, M., and de Capitani, C., 2012, Origin of pseudotachylites in slow creep experiments: Earth and Planetary Science Letters, v. 355–356, p. 299–310, doi:10.1016/j.epsl.2012.09.004.

Pennacchioni, G., 2005, Control of the geometry of precursor brittle structures on the type of ductile shear zone in the Adamello tonalites, Southern Alps (Italy): Journal of Structural Geology, v. 27, p. 627–644, doi:10.1016/j.jsg.2004.11.008.

Price, N.A., Johnson, S.E., Gerbi, C.C., and West, D.P., 2012, Identifying deformed pseudotachylyte and its influence on the strength and evolution of a crustal shear zone at the base of the seismogenic zone: Tectonophysics, v. 518–521, p. 63–83, doi:10.1016/j.tecto.2011.11.011.

Ray, S.K., 1999, Transformation of cataclastically deformed rocks to pseudotachylyte by pervasion of frictional melt: Inferences from clast-size analysis: Journal of Structural Geology, v. 301, no. 3–4, p. 283–304.

Reimold, W.U., 1998, Exogenic and endogenic breccias: a discussion of major problematics: Earth-Science Reviews, v. 43, no. 1, p. 25–47.|

Reimold, W.U., and Gibson, R.L., 2005, "Pseudotachylites" in large impact structures, *in* Koeberl, C., and Henkel, H., eds., Impact Tectonics: Springer, p. 1–53.

Rolandone, F., Bürgmann, R., and Nadeau, R.M., 2004, The evolution of the seismic-aseismic transition during the earthquake cycle: Constraints from the time-dependent depth distribution of aftershocks: Geophysical Research Letters, v. 31, p. L23610, doi:10.1029/2004GL021379.

Schwarzkopf, L., Schmincke, H.-U., and Troll, V., 2001, Pseudotachylite on impact marks of block surfaces in block-and-ash flows at Merapi volcano, central Java, Indonesia: International Journal of Earth Sciences, v. 90, no. 4, p. 769–775, doi:10.1007/s005310000171.

Shaw, C.A., and Allen, J.L., 2007, Field rheology and structural evolution of the Homestake shear zone, Colorado: Rocky Mountain Geology, v. 42, no. 1, p. 31–56, doi:10.2113/gsrocky.42.1.31.

Shaw, C.A., Snee, L.W., Selverstone, J., and Reed, J.C., Jr., 1999, $^{40}Ar/^{39}Ar$ thermochronology of Mesoproterozoic metamorphism in the Colorado Front Range: The Journal of Geology, v. 107, p. 49–67, doi:10.1086/314335.

Shaw, C.A., Karlstrom, K.E., Williams, M.L., Jercinovic, M.J., and McCoy, A.M., 2001, Electron-microprobe monazite dating of ca. 1.71–1.63 Ga and ca. 1.45–1.38 Ga deformation in the Homestake shear zone, Colorado: Origin and early evolution of a persistent intracontinental tectonic zone: Geology, v. 29, p. 739–742, doi:10.1130/0091-7613(2001)029<0739:EMMDOC>2.0.CO;2.

Shaw, C.A., Karlstrom, K.E., McCoy, A., Williams, M.L., Jercinovic, M.J., and Dueker, K., 2002, Proterozoic shear zones in the Colorado Rocky Mountains: From continental assembly to intracontinental reactivation, *in* Lageson, D., ed., Science at the Highest Level: Geological Society of America Field Guide 3, p. 1–16.

Shaw, C.A., Heizler, M.T., and Karlstrom, K.E., 2005, $^{40}Ar/^{39}Ar$ thermochronologic record of 1.45–1.35 Ga intracontinental tectonism in the southern Rocky Mountains: Interplay of conductive and advective heating with intracontinental deformation, *in* Karlstrom, K.E., and Keller, G.R., eds., The Rocky Mountain Region—An Evolving Lithosphere: Tectonics, Geochemistry, and Geophysics: Washington, D.C., Geophysical Monograph, American Geophysical Union, p. 163–184.

Sibson, R.H., 1973, Interactions between temperature and pore-fluid pressure during earthquake faulting and a mechanism for partial or total stress relief: Nature, v. 243, p. 66–68, doi:10.1038/physci243066a0.

Sibson, R.H., 1975, Generation of pseudotachylyte by ancient seismic faulting: Geophysical Journal of the Royal Astronomical Society, v. 133, p. 191–213.

Sibson, R.H., 1984, Roughness at the base of the seismogenic zone: Contributing factors: Journal of Geophysical Research, v. 89, no. B7, p. 5791–5799, doi:10.1029/JB089iB07p05791.

Silver, L.T., 1965, Mazatzal orogeny and tectonic episodicity: Geological Society of America Special Paper, v. 82, p. 185–186.

Silver, L.T., 1984, Observations on the Precambrian evolution of northern New Mexico and adjacent regions: Geological Society of America Abstracts with Programs, v. 16, p. 256.

Silver, L.T., Bickford, M.E., Van Schmus, W.R., Anderson, J.L., Anderson, T.H., and Medaris, L.G., Jr., 1977, The 1.4–1.5 b.y. transcontinental anorogenic plutonic perforation of North America: Geological Society of America Abstracts with Programs, v. 9, p. 1176–1177.

Smith, S.A.F., Bistacchi, A., and Mitchell, T., Mittempergher, Di Toro, G., 2013, The structure of an exhumed intraplate seismogenic fault in crystalline basement: Tectonophysics, v. 599, p. 29–44; doi:10.1016/j.tecto.2013.03.031.

Spray, J., 1987, Artificial generation of pseudotachylyte using friction welding apparatus: Simulations of melting on a fault plane: Journal of Structural Geology, v. 9, p. 49–60, doi:10.1016/0191-8141(87)90043-5.

Spray, J., 1995, Pseudotachylyte controversy: Fact or friction?: Geology, v. 23, p. 1119–1122, doi:10.1130/0091-7613(1995)023<1119:PCFOF>2.3.CO;2.

Spray, J., 1997, Superfaults: Geology, v. 25, p. 579–582, doi:10.1130/0091-7613(1997)025<0579:S>2.3.CO;2.

Spray, J., 2005, Evidence for melt lubrication during large earthquakes: Geophysical Research Letters, v. 32, p. L07301, doi:10.1029/2004GL022293.

Spray, J.G., 2010, Frictional melting processes in planetary materials: From hypervelocity impact to earthquakes: Annual Review of Earth and Planetary Sciences, v. 38, p. 221–254, doi: 10.1146/annurev.earth.031208.100045.

Spray, J., and Thompson, L.M., 1995, Friction melt distribution in a multi-ring impact basin: Nature, v. 373, p. 130–132, doi:10.1038/373130a0.

Swanson, M.T., 1992, Fault structure, wear mechanisms and rupture processes in pseudotachylyte generation: Tectonophysics, v. 204, no. 3–4, p. 223–242, doi:10.1016/0040-1951(92)90309-T.

Swanson, M.T., 2006, Pseudotachylyte-bearing strike-slip faults in mylonitic host rocks, Fort Foster Brittle Zone, Kittery, Maine, *in* Abercrombie, R., McGarr, A., Di Toro, G., and Kanamori, H., eds., Earthquakes: Radiated Energy and the Physics of Faulting: American Geophysical Union Geophysical Monograph Series 170, p. 167–179.

Trepmann, C.A., and Stockhert, B., 2003, Quartz microstructures developed during non-steady state plastic flow at rapidly decaying stress and strain rate: Journal of Structural Geology, v. 25, p. 2035–2051, doi:10.1016/S0191-8141(03)00073-7.

Tuffen, H., and Dingwell, D., 2005, Fault textures in volcanic conduits: Evidence for seismic trigger mechanisms during silicic eruptions: Bulletin of Volcanology, v. 67, p. 370–387, doi:10.1007/s00445-004-0383-5.

Tweto, O., 1974, Geologic map and sections of the Holy Cross quadrangle, Eagle, Lake, Pitkin, and Summit Counties, Colorado: U.S. Geological Survey Map I-830, scale 1:24,000.

Tweto, O., and Lovering, T.S., 1977, Geology of the Minturn 15-minute quadrangle, Eagle and Summit counties, Colorado: U.S. Geological Survey Professional Paper 956, 96 p.

Tweto, O., and Sims, P.K., 1963, Precambrian ancestry of the Colorado mineral belt: Geological Society of America Bulletin, v. 74, p. 991–1014, doi:10.1130/0016-7606(1963)74[991:PAOTCM]2.0.CO;2.

Tweto, O., Moench, R.H., and Reed, J.C., Jr., 1978, Geologic map of the Leadville 1° × 2° quadrangle, northwestern Colorado: U.S. Geological Survey Map I-999, scale 1:250,000.

Wallace, A.R., and Blaskowski, M.J., 1989, Geologic map of the Mount Jackson quadrangle and the eastern part of the Crooked Creek Pass quadrangle, Eagle County, Colorado: U.S. Geological Survey, Miscellaneous Investigation Series Map I-1909, scale 1:24,000.

Wallace, A.R., Blaskowski, M.J., and Pearson, R.C., 1986, Geologic map of the Holy Cross Wilderness, Eagle, Pitkin, and Lake counties, Colorado: U.S. Geological Survey Miscellaneous Field Studies Map 1841-A, scale 1:24,000.

Whitmeyer, S.J., and Karlstrom, K.E., 2007, Tectonic model for the Proterozoic growth of North America: Geosphere, v. 3, p. 220–259, doi:10.1130/GES00055.1.

Manuscript Accepted by the Society 17 July 2013

Printed in the USA